R-06-27

Bedrock transport properties
Data evaluation and retardation model

Preliminary site description
Laxemar subarea – version 1.2

Johan Byegård, Eva Gustavsson, Geosigma AB

Eva-Lena Tullborg, Terralogica AB

June 2006

Svensk Kärnbränslehantering AB
Swedish Nuclear Fuel
and Waste Management Co
Box 5864
SE-102 40 Stockholm Sweden
Tel 08-459 84 00
+46 8 459 84 00
Fax 08-661 57 19
+46 8 661 57 19

ISSN 1402-3091
SKB Rapport R-06-27

Bedrock transport properties
Data evaluation and retardation model

Preliminary site description
Laxemar subarea – version 1.2

Johan Byegård, Eva Gustavsson, Geosigma AB

Eva-Lena Tullborg, Terralogica AB

June 2006

Keywords: Retardation model, Transport properties, Laxemar, Fracture mineralogy, Diffusivity, Porosity, Sorption.

Abstract

This report presents the site descriptive model of transport properties developed as a part of the Laxemar 1.2 site description. The main parameters included in the model, referred to as retardation parameters, are the porosity and diffusivity, and the sorption coefficient K_d, so far mainly from the rock matrix. The model is based on the presently available site investigation data, mainly obtained from laboratory investigations of core samples from boreholes within the Laxemar subarea. The modelling is a first attempt, based on limited data, to obtain a description of the retardation parameters. Further refinement of the model is foreseen when more data becomes available for future versions of the Laxemar site description.

The modelling work included descriptions of rock mass geology, the fractures and fracture zones, the hydrogeochemistry and also the available results from the site specific porosity, sorption and diffusivity measurements. The description of the transport-related aspects of the data and models presented by other modelling disciplines is an important part of the transport description. In accordance with the strategy for the modelling of transport properties, the results are presented as a retardation model, in which a summary of the transport data for the different geological compartments is given. Porosity and formation factors have been measured for the major rock types using site specific materials from the Laxemar area. Mean values for the major rock types have been obtained in the range of 0.26–0.36 vol-% for the porosity and 3.6×10^{-5}–1.4×10^{-4} for the formation factor. Preliminary sorption coefficients have been extracted from the investigation programme, using Ävrö granite sampled in KLX03A at 522.61–523.00 m depth. Sorption coefficients, K_d values, have been measured for Cs(I), Sr(II), Ni(II), Ra(II) and Am(III). The obtained values correspond with some exceptions to the values in the database developed for the previous SKB SR-97 performance assessment /Carbol and Engkvist 1997/.

Ävrö granite and quartz monzodiorite are identified as the rock types dominating the main rock domains identified and described in the site descriptive model of the bedrock geology. However, relatively large parts of the rock consist of altered rock with an increased open fracture frequency. This implies that transport in open fractures to a larger extent takes place in altered parts than in fresh parts of the rock. Mapped crush zones shows an overlap in transmissivity with the single factures; there is a grey zone between what is defined as single fractures and minor zones for transport modelling purpose. For the fracture mineralogy, it is found that the hydraulically conductive structures are commonly associated with the presence of clay minerals. The mineralogy of the different fracture coatings cannot be correlated to their corresponding host rock type. The descriptions of bedrock geology and fracture mineralogy are used as a basis for identifying a set of fracture types considered typical for the boreholes in the Laxemar subarea. Four fracture types are identified and described in terms of geometry (thicknesses of different layers) and retardation parameters. Due to the uncertainties in definition of minor deformation zones and lack of site data, no parameterisation of these has been performed.

The hydrochemistry in the Laxemar subarea is characterised by fresh water (of present meteoric and glacial meltwater origins), which at depth interacts with deep saline groundwater. Within the transport program four different groundwater types have been identified for use in the laboratory measurements. The water types have been selected to suit both the Simpevarp/Laxemar and Forsmark sites. These waters are: (I) fresh diluted Ca-HCO_3 water, (II) groundwater with marine character (Na-(Ca)-Mg-Cl, 5,000 mg/L Cl), (III) groundwater of Na-Ca-Cl type (8,800 mg/L Cl), (IV) groundwater of very high salinity (Ca-Na-Cl type

water with Cl content of 45,000 mg/L). For the batch sorption measurements carried out on the Laxemar material, groundwaters of type I, and III (and for a smaller number of samples also type IV) have been used.

Finally in the report, tables describing the retardation parameters assigned to each major rock type and each fracture type are presented. These data tables constitute the Laxemar 1.2 retardation model, which is the main delivery from the site descriptive transport modelling to Safety Assessment concerning quantitative, site specific information on the retardation parameters.

Sammanfattning

I denna rapport redovisas den beskrivande modellen av retardationsparametrarna, den s k retardationsmodellen, vilken är utgör en del av platsbeskrivningen Laxemar 1.2. De huvudsakliga parametrarna som inkluderats i modellen är porositet, diffusivitet och sorptionskoefficienten K_d, vilka hittills uppmätts i prover från bergmatrisen. Modellen baseras på i nuläget tillgängliga platsundersökningsdata, huvudsakligen erhållna från laboratorieundersökningar av borrkärneprover från borrhål i Laxemarområdet. Modelleringen är ett första försök att utifrån den begränsade mängden tillgängliga data ta fram en beskrivning av de aktuella retardationsparametrarna. Mer detaljerade modeller kan förväntas i de framtida platsbeskrivningarna då större mängder platsspecifika data kommer att vara tillgängliga.

Modelleringsarbetet innehåller beskrivningar av berggrundsgeologin, sprickor och deformationszoner, hydrogeokemiska data, och även de i nuläget tillgängliga data från platsspecifika mätningar av porositet, diffusivitet och sorptionskoefficienter. Beskrivningar av transportrelaterade aspekter av data och modeller som utvecklats av andra ämnesområden inom platsmodelleringen är också en viktig del av transportbeskrivningen. I enlighet med strategin för modelleringen av transportegenskaper presenteras resultaten i form av en retardationsmodell, i vilken en summering ges av transportdata för de olika geologiska enheterna.

Porositeter och formationsfaktorer har mätts för huvudbergarterna med platsspecifika prover från Laxemarområdet. De medelvärden för porositet för huvudbergarterna som uppmätts ligger i intervallet 0,26–0,36 vol-%. Motsvarande medelvärdesintervall för formationsfaktorn är $3{,}6\times10^{-5}$–$1{,}4\times10^{-4}$. Preliminära sorptionskoefficienter har beräknats på basis bergartsprov av Ävrögranit från KLX03 på 522,61–523,00 m djup. K_d-värden för Cs(I), Sr(II), Ni(II), Ra(II) och Am(III) för två olika grundvatten (typ I och typ III) har beräknats och överrensstämmer i huvudsak med SKB:s databas från den tidigare säkerhetsanalysen SR-97 /Carbol och Engkvist 1997/.

Ävrögranit och kvartsmonzodiorit har identifierats som huvudbergarter i de bergdomäner som beskrivits i den platsbeskrivande geologiska modellen. Dock utgörs relativt stora delar av berggrunden av omvandlat bergmaterial med en ökad frekvens av öppna sprickor. Detta medför att transport i öppna sprickor till en större del sker i omvandlat än i ej omvandlat berg. Vad beträffar sprickmineralogin kan det konstateras att hydrauliskt ledande strukturer vanligtvis karaktäriseras av närvaro av lermineral. Sprickornas mineralogiska sammansättning går dock inte att enkelt korrelera till de huvudbergarter som dessa sprickor går igenom. Beskrivningen av berggrundsgeologin och sprickmineralogin har använts för att identifiera ett antal typsprickor som anses representera berget i Laxemarområdet. Fyra olika sprick-typer har identifierats och beskrivits i termer av geometrier (de olika skiktens tjocklekar) och retardationsparametrar. På grund av oklarheter i definitionen av mindre deformationszoner och bristen på platsdata har ingen parameterisering gjorts av dessa.

Grundvattenkemin inom delområde Laxemar karakteriseras av sött vatten som på större djup blandas med ett salint grundvatten med lång uppehållstid i berget. Delar av det söta vattnet har ett glacialt ursprung. Inom transport programmet har fyra olika vattentyper valts ut för laboratorieförsöken. Dessa vatten skall representera möjliga vatten på förvarsdjup samt möjliga extremer inom både Simpevarp/Laxemar- och Forsmarksområdena. Dessa vattentyper är: (I) sött vatten av Ca-HCO_3-typ, (II) grundvatten av marin karaktär (Na-(Ca)-Mg-Cl, 5 000 mg/L Cl), (III) grundvatten av Na-Ca-Cl-typ (8 800 mg/L Cl), (IV) grundvatten med mycket hög salthalt (Ca-Na-Cl-typ med Cl-innehåll på ca 45 000 mg/L).

För de sorptionsstudier som utförs på Laxemarmaterial har vattentyp I och III används, samt för ett mindre antal prover även vattentyp IV.

Rapporten avslutas med tabeller som beskriver retardationsparametrar har givits för varje huvudbergart och för varje spricktyp. Dessa tabeller utgör retardationsmodell Laxemar 1.2 och är alltså den huvudsakliga leveransen från den platsbeskrivande transportmodelleringen till Säkerhetsanalys vad gäller kvantitativ platsspecifik information om retardations-parametrarna.

Contents

1 Introduction

1.1 Background

The Swedish Nuclear Fuel and Waste Management Company (SKB) is conducting site investigations at two different locations, the Forsmark and Oskarshamn areas, with the objective of siting a geological repository for spent nuclear fuel. The results from the investigations at the sites are used as a basic input to the site descriptive modelling.

A Site Descriptive Model (SDM) is an integrated description of the site and its regional setting, covering the current state of the geosphere and the biosphere as well as ongoing natural processes of importance for long-term safety. The SDM shall summarise the current state of knowledge of the site, and provide parameters and models to be used in further analyses within Safety Assessment, Repository Design and Environmental Impact Assessment. The present report is produced as a part of the version 1.2 modelling of the Laxemar subarea (the L1.2 modelling, for short). A similar report describing the retardation parameters obtained from boreholes within the Simpevarp subarea /Byegård et al. 2005a/, which is also within the Oskarshamn site investigation area, was presented in connection with the Simpevarp 1.2 SDM /SKB 2005/.

The process of site descriptive modelling of transport properties is described by /Berglund and Selroos 2004/. Essentially, the description consists of three parts:

- Description of rock mass and fractures/deformation zones, including relevant processes and conditions affecting radionuclide transport; the description should express the understanding of the site and the evidence supporting the proposed model.
- Retardation model: Identification and description of "typical" rock materials and fractures/deformation zones, including parameterisation.
- Transport properties model: Parameterisation of the 3D geological model and assessment of understanding, confidence and uncertainty.

The methods used within the transport programme produce primary data on the retardation parameters, i.e. the porosity, θ_m, the effective diffusivity, D_e, and the linear equilibrium sorption coefficient, K_d. These retardation parameters are evaluated, interpreted and presented in the form of a retardation model; the strategy for laboratory measurements, data evaluation and development of retardation models is described by /Widestrand et al. 2003/. In the three-dimensional modelling, the retardation model is used to parameterise the various geological "elements" (rock mass, fractures and deformation zones) in the site-descriptive geological model.

The present report deals with the development of the retardation model only. This means that it describes the considerations involved in the extraction of data from the available site specific database, and the construction of the retardation model using these data. Additional considerations and implications associated with the application of this retardation model in the broader L1.2 SDM transport modelling perspective are discussed in /Crawford 2006/. Thus, the present report is focused on data evaluation and retardation model development, whereas the L1.2 transport model, including flow-related transport parameters and analysis of retardation along flow paths, is presented /Crawford 2006/.

1.2 Conceptual model

The conceptual model underlying the site descriptive transport modelling is based on a description of solute transport in discretely fractured rock. Specifically, the fractured medium is viewed as consisting of mobile zones, i.e. fractures and deformation zones where groundwater flow and advective transport take place, and immobile zones in rock mass, fractures and deformation zones where solutes can be retained, i.e. be removed, temporally or permanently, from the mobile water /Berglund and Selroos 2004/. In the safety assessment framework that provides the basis for identification of retention parameters in the site descriptive models, retention is assumed to be caused by diffusion and linear equilibrium sorption. These processes are reversible and are here referred to as retardation processes.

The conceptualisation outlined above implies that radionuclide transport takes place along flow paths consisting of connected "subpaths" in fractures and deformation zones of different sizes. In this model, advection is the dominant process for moving the radionuclides in the transport direction, whereas the main role of diffusion is to remove the solutes from the mobile zone and transport them within the immobile zones.

It should be noted that this conceptual model and the present methodology for site descriptive modelling in general are based on experiences from the Äspö Hard Rock Laboratory (Äspö HRL), primarily the Tracer Retention Understanding Experiment (TRUE) project /Winberg et al. 2000, Poteri et al. 2002/ and the Äspö Task Force on modelling of groundwater flow and transport of solutes, e.g. /Dershowitz et al. 2003/, which are not necessarily fully applicable to the transport conditions at the Laxemar site. This is to say that the modelling strategy and the basic conceptual model could be revised as a result of experiences gained in the site descriptive modelling.

1.3 This report

The aim of the present report is to give a description of the development L1.2 retardation model, and to give the background of the data that are used for the justification of the retardation model. Thus, the report focuses primarily on the first and second bullet points in the strategy outlined in Section 1.1. The data and models used as input to the modelling are described in Chapter 2, including the inputs from other modelling disciplines. Chapter 3 presents the evaluation of Transport data, whereas the resulting model is described in Chapter 4. Finally, Chapter 5 contains a brief discussion on the implications of the results for the continued investigations and modelling.

For the L1.2 model version, the major concern was to use data strictly from the Laxemar subarea and not to include the previously presented /Byegård et al. 2005a/ data from the Simpevarp subarea. However, a comparison between the Simpevarp and Laxemar retardation data is presented in /Crawford 2006/. The main exception is that results from laboratory measurements on fracture materials from both Simpevarp and Laxemar have been included in the present report. The decision to use all fracture materials data is based on the fact that the fracture minerals found are the same in both subareas.

This is partly true for the Äspö material as well, but the nomenclature and groundwater compositions used in the laboratory studies of the Äspö materials differed. Therefore, no data have been imported from Äspö in this model version. Despite the similarities in rock types and fracture mineral compositions, the parameterisation of the Laxemar subarea differs from the model of the Simpevarp subarea. This due to differences in fracture frequencies (some fracture types are more common on Laxemar and vice versa), the larger extent of wall rock alteration visible in the Simpevarp subarea, and the differences in rock type distributions.

2 Description of input data

2.1 Summary of available data

The input data to the Laxemar 1.2 modelling (L1.2 for brevity) of transport properties are summarised in Table 2-1. The available site investigation data on transport properties data are summarised by /Börjesson and Gustavsson 2005/, /Thunehed 2005ab/ and /Löfgren and Neretnieks 2005/. The important input from the combined geological/hydrogeochemical interpretations of fracture mineralogy and wall rock alteration data is provided by /Drake and Tullborg 2004, 2005, 2006ab/.

As shown in Table 2-1, other geological, hydrogeological and hydrogeochemical inputs were obtained from the SDM report /SKB 2006a/, i.e. from draft versions of the relevant chapters, and from the geological /Wahlgren et al. 2005/, hydrogeochemical /SKB 2006b/ and hydrogeological /Forssman et al. 2005, Rhén et al. 2006/ data and modelling reports. These inputs are further detailed below.

Table 2-1. Available data on transport properties and input data from other disciplines, and their handling in Laxemar 1.2 (L1.2).

Available primary data, data specification	Ref	Usage in L1.2 analysis/modelling
Transport properties data		
Resistivity measurements and determination of formation factors on samples from KLX02 and KLX04	P-05-19 P-05-75 /Löfgren 2001/	Assignment of diffusion parameters.
Formation factor logging in situ by electrical methods in KLX03 and KLX04	P-05-105	Assignment of diffusion parameters.
Laboratory data from the site investigation programme from the transport properties of the rock	P-05-106	Assignment of porosity and diffusion parameters.
Input from other disciplines		
Geological data and description:		
– lithology and mineralogy of identified rock types	SDM chapter R-05-69	Identification of site-specific rock types, fractures and fracture zones and properties of site-specific geological materials, as a basis for the Retardation model and the descriptive Transport model.
– fracture mineralogy	P-04-250 P-05-174 P-06-01 P-06-02	
Hydrogeological data and description	SDM chapter P-05-241 R-06-22	Identification of conductive fractures and correlations between fracture types and hydraulic properties.
Hydrogeochemical description	SDM chapter R-06-12	Identification of site-specific hydrochemical water types.

2.2 Data and models from other disciplines

2.2.1 Geology

The summary and evaluation of geological data of relevance for the transport modelling (see below) is based on the L1.2 geological description, as presented in Chapter 5 of the L1.2 SDM report /SKB 2006a/, and the associated models and databases. Specifically, the geological models were delivered in Nov 2005, and a draft version of the geological description (i.e. Chapter 5 in the SDM report) was made available for the Transport modelling.

Rock types

Igneous rocks belonging to the c. 1,800 Ma generation of the Transscandinavian Igneous Belt (TIB) dominate in the Laxemar regional and local scale model areas. As described in /Wahlgren et al. 2005/, magma mixing and mingling and diffuse contact relationships is a characteristic feature of these rocks, which show compositions varying from true granites to quartz monzodiorite.

Two rock types dominate the Laxemar subarea: Ävrö granite in the north and middle part and quartz monzodiorite in the south and southwest and in two minor areas in the north eastern part of area. The dioritoid, which together with Ävrö granite and quartz monzodiorite constitutes the major rock types in the Simpevarp subarea, is considered as a minor rock type in the Laxemar subarea. The quartz monzodiorite is equigranular with quartz monzodioritic to granodioritic composition, while the Ävrö granite is medium grained and usually porphyritic in texture with varying compositions from granite to quartz monzodiorite.

The properties and characteristics of these rock types are given in tables in /Wahlgren et al. 2005/. Surface outcrop samples indicate that the compositional variations of the Ävrö granite have a systematic distribution within the Laxemar subarea showing granitic to granodioritic (quartz rich) composition in the central parts and quartz monzodioritic (quartz poor) composition in the southern part of the area. The available information on the spatial distributions of these two types at depth is limited.

Minor rock types, most of which are additional varieties of rocks belonging to the TIB suite, occur as dikes, lenses and xenoliths. These consist of fine-grained granite, fine-grained dioritoid, medium- to coarse-grained granite, pegmatite, and diorite to gabbro. Of the subordinate rock types, fine-grained granite is the most frequent with a relatively regular distribution within the two major rock types. There is a notable concentration of diorite to gabbro as well as elongated bodies of fine-grained dioritoid, in the area between the Ävrö granite and the quartz monzodiorite, see Figure 2-1 /Wahlgren et al. 2005/.

Rock domains

From the geological map and the borehole loggings it is obvious that, on a detailed scale, there is a mix of rock types. For the lithological modelling of the area, the concept of rock domains is introduced in order to facilitate the development of a three-dimensional geological model. The major components building up the rock domains are the following:

RSMA01 = dominantly Ävrö granite.

RSMD01 = dominantly quartz monzodiorite.

RSMBA = characterized by a mixture of dominantly Ävrö granite and fine-grained dioritoid.

RSMM01 = characterized by a high frequency of minor bodies to small enclaves of diorite to gabbro in, particularly, Ävrö granite and quartz monzodiorite.

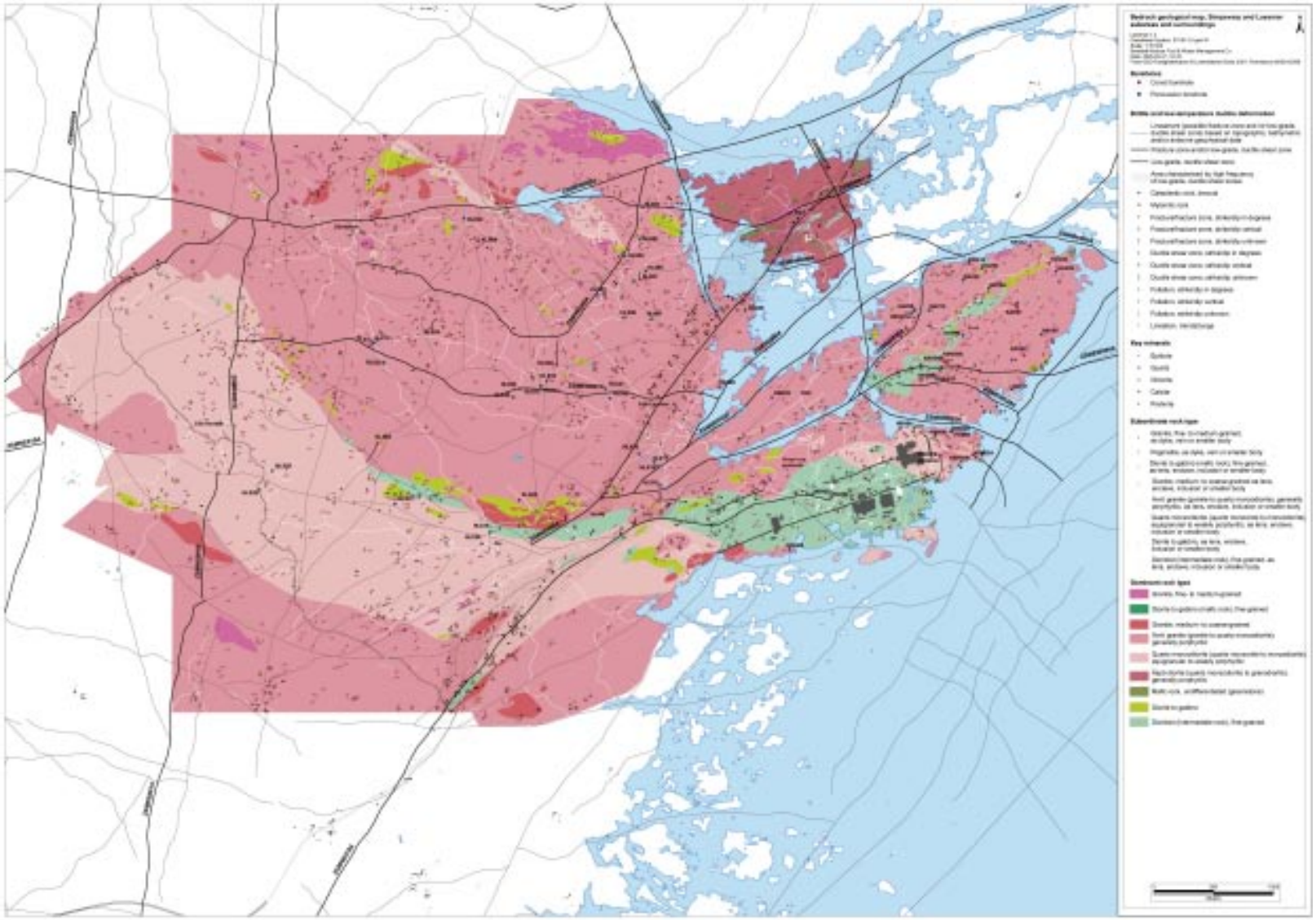

Figure 2-1. *Map of bedrock geology in the Laxemar and Simpevarp subareas and their surroundings /Wahlgren et al. 2005/.*

The two rock domains RSMA01 and RSMD01 dominate the local scale model volume in the Laxemar subarea, RSMA01 in the northern to north-eastern part and RSMD01 in the southern to south-western parts. To a minor extent rock domain RSMM01 and rock domains of type RSMBA appear as lenses, in particular between RSMA01 and RSMD01, cf Figure 2-2 /Wahlgren et al. 2005/. Fine-grained granite, which is a minor rock type with usually a higher hydraulic conductivity than the major rock types (cf Chapter 8 in the SDM L1.2 report /SKB 2006a/), is included as a minor constituent in the different rock domains.

In the geological modelling, the rock domains are assigned properties, comprising mineralogical composition, grain size, texture, density, porosity, etc. The lithological model and the parameters assigned to each rock domain are summarised in Appendix 5 of the SDM L1.2 report; the proportions of different rock types within the rock domains are illustrated in Figures 3-7 to 3-13 in /Wahlgren et al. 2005/.

Table 2-2 shows the volume of altered rock compared to the fresh rock in rock domain RSMA01 and RSMD01 at the Laxemar subarea. Four different degrees of alteration are used in the core logs: faint, weak, medium and strong. As indicated by the figures in the table, relatively large parts of the RSMA01 and RSMD01 are affected by this alteration. However, variations in intensity between the boreholes are recorded.

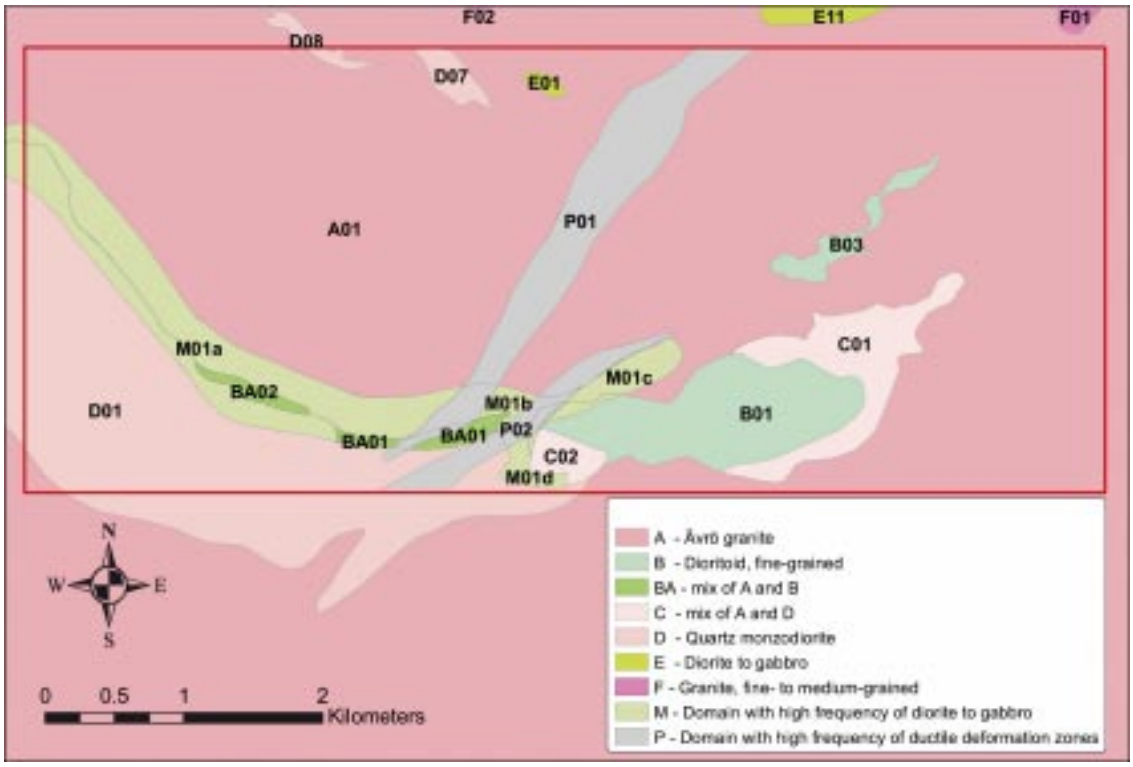

Figure 2-2. *Two-dimensional local model of rock domains in the Laxemar subarea (to the west on the map); see /Wahlgren et al. 2005/ for a detailed description.*

The cause of the observed red-staining of the rock is hydrothermal alteration which has resulted in saussuritisation of plagioclase, breakdown of biotite to chlorite and oxidation of Fe(II) to form hematite, mainly present as micro-grains giving the red colour. However, there is not always a perfect correspondence between the extent of hydrothermal alteration and the extent of red-staining /Drake and Tullborg 2006ab/. The altered parts of the rock can be assumed to have different transport properties due to, e.g. lower biotite content and partly higher content of sericite and illite (influencing the sorption capacity), and usually higher porosity and possible also changed structure of the porosity (influencing the diffusivity). It is therefore an important consideration that the major rock types in the two dominating rock domains show alteration (rated as weak/medium/strong) in at least 8% of the rock mass, and in most cases more.

Table 2-2. Alteration/oxidation and saussiritisation in the different rock domains. The alteration is classified into four classes: faint, weak, medium and strong.

Rock domain	Fresh (%)	Faint (%)	Weak (%)	Medium (%)	Strong (%)
RSMA01[A]	67–75	11–20	8–13	0–5	0
Dominantly Ävrö granite Mainly oxidation					
RSMD01[B]	68	20	12	1	0
Dominantly quartz monzodiorite Mainly saussiritisation					

A) RSMA01 is mainly based on KLX02 and KLX04 data.

B) RSMD01 is mainly based on KLX03 data.

2.2.2 Fractures and deformation zones

An overview of rock types, alteration and frequencies of sealed and open fractures in the Laxemar boreholes are given in the L1.2 SDM report /SKB 2006a/. These results show that the frequency of sealed fractures does not always correlate with the frequency of open fractures.

Fracture minerals are initially documented during the mapping of the drill core according to the boremap programme, which forms an integral part of the site characterisation protocol. Based on this information, fracture fillings are further selected for more detailed studies, which involve X-ray diffractometry for identification of clay minerals and fault gouge materials, and microscopy of fracture fillings. Suitable samples are also selected for isotopic analyses of calcites and pyrites, and a smaller number of fracture fillings from water conducting fractures are sampled for U series analyses.

The most common fracture minerals at the Laxemar site as well as at the Simpevarp site, are chlorite and calcites, which occur in several different varieties and are present in most of the open fractures. Other common minerals are epidote, laumontite, quartz, adularia (low-temperature K-feldspar), fluorite, hematite, prehnite and pyrite. A Ba-zeolite named harmotome has been identified in some fractures and apophyllite has been identified in a few diffractograms. Gypsum (small amounts) has been found in some fractures in KLX03 and KLX06 /Ehrenborg and Dahlin 2005ab/. A compilation of the available fracture mineralogy results is presented in the Laxemar 1.2 background report for geology. /Wahlgren et al. 2005/

The most frequently found clay mineral, in addition to chlorite, is corrensite (mixed layer chlorite/smectite or chlorite/vermiculite clay) where the smectite or vermiculite layers are swelling. Other identified clay minerals are illite, mixed-layer illite/smectite (swelling) and a few observations of smectites. In the first boreholes logged (at Simpevarp) there was a general tendency towards clay minerals being underrepresented in the core loggings, mainly due to difficulties in determining clay minerals macroscopically when mixed with other minerals but also due to possible loss of loose and soft phases during the drilling. It looks like this under-representation is much less evident in the KLX03 and KLX04 loggings. However, loss of material during drilling is still difficult to correct for.

Conclusions of importance for the transport modelling, mainly summarised from results in /Drake and Tullborg 2004, 2005, 2006ab/ are:

1) In accordance with earlier findings by /Munier 1993/ it has not so far been possible to relate different fracture minerals to different fracture orientations, but it is possible that certain key minerals like laumontite, prehnite or gypsum later will be possible to relate to orientations as the core mapping database will evolve.
2) The sequence of mineral paragenesis shows the transition from epidote facies in combination with ductile deformation, over to brittle deformation and breccia sealing during prehnite facies and subsequent zeolite facies. An even lower formation temperature series indicates that the fractures were initiated relatively early in the geological history of the host rock and have been reactivated during several different periods of various physiochemical conditions.
3) The locations of the hydraulically conductive fractures and minor deformation zones are often associated with identified deformation zones, produced by brittle reactivation of earlier ductile precursors or hydrothermally sealed fractures
4) The outermost coatings along the hydraulically conductive fractures consist of chlorite together with calcite, clay minerals, usually illite and mixed layer clays (corrensite = chlorite/smectite and illite/smectite), and minor grains of pyrite.

The detailed fracture filling studies can, for practical reasons, only be carried out on a small number of samples, whereas the statistical overview can be obtained from Boremap data.

For the transport modelling the single fractures constituting the transport pathways from a potentially broken canister to a fracture zone is the main focus. A central problem in establishing a retention properties model is how to identify and describe these fractures (or fracture types), which are well connected and large enough to have a dominant effect on flow and transport near the repository, but also are small enough to not be identified as minor zones. In the present model version, crush zones have been excluded from the statistics of fractures and fracture mineralogy.

A crush zone is defined as a section of the core with a number of open fractures separated by a distance less than 5 cm of unfractured rock; this is the definition used within the Boremap core logging and crush zones should not be considered as deterministic zones. Whether it is correct to exclude the mapped crush zones in the statistics needs to be further evaluated together with the geological and hydrogeological teams within the scope of forthcoming model versions. Especially for Laxemar and Simpevarp, there seems to be an overlap in size and transmissivity between single fractures and crush zones and the question is if, or not, all crush zones should be defined as minor deformation zones in the transport modelling perspective.

The total numbers of fractures in the boreholes (KLX02, KLX03, KLX04, KLX05 and KLX06) are on the order of 3,000 to 6,000 fractures/1,000 m borehole. Only 9 to 37% of these fractures are mapped as open (cf Table 2-3). This number is larger for borehole KLX02 (68%) but this borehole is drilled with a less sophisticated technique (single instead of triple tube) which may at least partly explain its higher portion of open fractures. Table 2-3 shows the total number of fractures in the different boreholes and the number of fractures that can be correlated to a flow log anomaly where the transmissivity is 10^{-9}–10^{-7} m/s. The fracture frequency at the Laxemar site is generally lower than at the Simpevarp site, although a large variation of fracture frequencies is observed in Laxemar.

Of the mapped open fractures a smaller portion (c 10–15%) is identified as water conducting in the measurements with the Posiva Flow Log (PFL), which so far has been carried out and evaluated in boreholes KLX02, KLX03 and KLX04 /Rhén et al. 2005/ The PFL measures the flow rate into or out of a limited section in the borehole. The features possible to identify by the flow log have transmissivities from 10^{-9} m/s and higher. In order to sort out the fractures of interest for the transport modelling, fractures with transmissivities up to 10^{-7} were selected (Table 2-3). One problem is that presumably a large part of the fractures mapped as open but not identified with the flow log have transmissivities large enough to be incorporated in the transport modelling.

Table 2-3. Total numbers of fractures in boreholes KLX02, KLX03, KLX04, KLX05 and KLX06. The percentages of open fractures correlated to PFL-anomalies are also given.

Borehole	Total number of fractures	Total number of open fractures	Total number of open fractures correlated to PFL-anomaly[A]	% PFL fractures related to total fracture frequency
KLX02	3,070	2,103 (68.5%)	205 (9.7%)	6.7%
KLX03	4,388	679 (15.5%)	81 (11.9%)	1.8%
KLX04	5,498	2,009 (36.5%)	287 (14.3%)	5.2%
KLX05	3,539	319 (9%)	No data	No data
KLX06	5,235	1,037 (19.8%)	No data	No data

A) PFL-anomaly = Posiva Flow Log anomalies showing transmissivities in the interval 10^{-9}–10^{-7} m²/s.

During the core mapping, the fractures have been given different confidence levels: certain, probable and possible. It seems to be the open fractures with confidence level “certain” that largely correspond to the fractures identified as water conducting, but as these only constitute 3–10% of all the open fractures it is likely that a portion of the fractures mapped as “probable” and “possible” should be considered as well. How to predict the portion of fractures that should be added to the PFL structures is a very difficult task and the problem is just addressed here. The parameterisation of the rock mass in between the fractures is dependent on assumptions made of the number of the open fractures that are included in the transport modelling as flowing structures, in that the rest of the fractures (the sealed and the open without flow) will contribute to the properties of the rock mass with a higher porosity and preferred diffusion pathways.

In conclusion:

1. Mapped crush zones show an overlap in transmissivity with the single factures; there is a grey area between what is defined as single fractures and minor deformation zones for transport modelling purposes.
2. There is most probably a portion of the mapped open fractures that are open to flow but with transmissivities below the PFL detection limit < 10^{-9} (which means that they are not identified in the PFL logs).
3. The incorporation of sealed fractures and a portion of the open but not transmissive fractures into the rock mass may speak in favour of adjustments of the rock mass properties cf for example /Löfgren and Neretnieks 2005/ found a 2–4 times larger formation factor in the fractured rock compared with sections without no identified fractures.

Concerning the fracture mineralogy based on the core loggings, it can be noted that no significant difference has been found between the open fractures in general and the open fractures identified with the flow log. Most of the fractures mapped as open contain chlorite and calcite (cf Table 2-4).

Other hydrothermal Al-silicates like prehnite, epidote and adularia are common but subordinate, and are not expected to give significant contributions to the sorption capacity. Clay minerals and hematite, in contrast, are expected to have comparably higher sorption capacities, and for this purpose the percentages of these fracture coatings in the open fractures are given as well. The Ca-zeolite laumontite (most common) and the Ba-zeolite harmotome (less common) are found in many fractures in the area, and zeolites may have high sorption capacities. Therefore, the frequency of laumontite has been evaluated as well (Table 2-4). Laumontite is important in the northern Laxemar area where it occurs in large volumes, e.g. in the "Mederhult zone" and in sealed fractures, but is only found as single observations in open fractures in the other Laxemar boreholes (KLX02, KLX04 and KLX05). On the other hand fractures sealed with porous and brittle minerals like laumontite may be reactivated and may also constitute important diffusion pathways.

The basic idea governing the selection of samples for the laboratory analysis has been to test the above listed five fracture coating types in terms of sorption, and after that, if possible, reduce the laboratory programme by concentrating on fewer coatings (perhaps to three or four coating types).

The figures presented in Table 2-4 give only the frequencies of fractures where the listed minerals have been found and not the amounts of the minerals in the fractures. Generally, hematite is always mapped and the amount in the fracture is easily overestimated due to the strong colouration produced by the ferric oxides/hydroxides. Clay minerals, in contrast, can be underrepresented, as already discussed, and the figures should be treated as an absolute minimum. Comparing to microscopy data, it is suggested that the combination of chlorite and calcite in the Boremap data sometimes are underestimated. This is probably due to difficulties in the identification of small amounts of calcite when it is mixed with a chlorite layer. Therefore, data for open fractures with chlorite is presented ± calcite in Table 2-4.

The percentages of fractures hosted in altered rock have been difficult to determine. At Simpevarp the redstaining was the obvious sign of alteration, but at Laxemar two different types of alteration are common; i.e. redstaining and saussuritization. Since most fractures in the area have hydrothermal minerals, they most probably also have hydrothermal alteration in the close wall rock. This alteration may not always have produced significant red-staining, and therefore some fractures may not have been mapped as altered even though they contain altered materials. Thin section studies /Drake and Tullborg 2004, 2006b/ support the presence of altered wall rock around the fractures coated with hydrothermal minerals. In parts of the KLX03 borehole, saussuritization is the most common alteration whereas in the other boreholes hydrothermal alteration visible as redstaining seems to be the most common. We therefore suggest that a significant part of the fractures have altered wall rock, cf Chapter 4.

Table 2-4. The percentages of open fractures coated with chlorite±calcite, hematite, clay minerals, gouge and laumontite and the same mineral coatings in open, transmissive fractures.

Frequency of minerals in open fractures	KLX02	KLX03	KLX04	KLX05	KLX06
Chlorite ± calcite	68.8	81.3	70.2	79.3	73.9
Hematite %	3.8	10.6	6.5	0.6	14.6
Clay minerals %	0.04	27.8	27.3	51.4	33.2
Laumontite %	0.1	0.15	0.55	0	4.6
Gouge %	0.05	1.2	0	0	0
Chlorite ± calcite % in fractures correlated to PFL-anomaly	65.8	71.6	67.9	No data	No data
Hematite % in fractures correlated to PFL-anomaly	5.8	8.6	4.2	No data	No data
Clay minerals % in fractures correlated to PFL-anomaly	0	22.2	22.0	No data	No data
Laumontite % in fractures correlated to PFL-anomaly	0	0	0	No data	No data
Gouge % in fractures correlated to PFL-anomaly	No data	No data	No data	No data	No data

For the sampling of fracture coatings for batch sorption measurements, the following approach has been taken: fracture coatings consisting of chlorite+calcite constitute the base, and fractures containing these two minerals in addition to other minerals of interest have been selected in order to determine the importance of some common fracture minerals. Therefore, five different coatings have been selected:

A. Chlorite + calcite

B. Chlorite+calcite ± adularia ± epidote ± prehnite ± pyrite

C. Chlorite+calcite+hematite±clay mineral

D. Chlorite+calcite+clay minerals

E. Chlorite+calcite+zeolite (laumontite + harmotome)

Fracture planes with coatings of type A and type C are illustrated in Figure 2-3.

Within the Geology programme, a number of deterministic deformation zones have been identified. In the Laxemar 1.2 geological model, 34 high confidence deformation zones where identified which where divided into regional and local major deformation zones. Within the Laxemar subarea a number of roughly E-W and N-S trending deformation zones have been identified. Prominent examples are the E-W trending Mederhult zone in the northern border of the Laxemar subarea and the deformation zone ZSMEW007 dividing the Laxemar area into a northern and a southern part. These zones have very long sections with severely altered rock with several sections of cataclasite and also dm-wide sections of poorly lithified fault gouge material consisting of crushed and altered rock fragments together with clay minerals and hematite.

For the modelling of retardation of radionuclides, the character of the minor deformation zones constitutes the link between the single fractures (discussed above) and large-scale zones like ZSMEW007. In order to ascribe realistic retardation capacities to the local minor deformation zones, the following approach has been adopted in the selection of samples: each zone is assumed to consist of one or several types of structure elements, consisting of altered wall rock. The conductive parts of the zones usually consist of several fractures and crush zones that can be referred to some of the fracture types listed above, or to a broader fault gouge-filled section. Therefore, four types of structure elements have been selected for porosity, diffusion and batch-sorption measurements, see Figure 2-4.

The present separation between single fractures and local minor deformation zones should be considered as a preliminary proposal, and will probably be the subject of discussions among hydrogeologists, geologists and transport modellers.

Figure 2-3. *Fracture planes with chlorite + calcite and prehnite (left), and chlorite + calcite and hematite (right).*

1. Fault gouge

Mineralogy: chlorite, clay minerals, hematite with fragments of quartz, epidote and calcite.

Strong fragmentations.

2. Chlorite

Mineralogy: chlorite and clay minerals.

3. Porous episyentic wall rock

Mineralogy: prehnite, adularia, quartz, calcite ± laumontite, epidote, hematite.

Partly mobilized quartz.

4. Cataclasite

Cataclasite with mylonitic banding. Mineralogy: epidote, adularia, quartz, hematite.

Figure 2-4. *Classification of structure elements building up the deformation zones in the Simpevarp and Laxemar subareas.*

2.2.3 Hydrogeochemistry

Conceptualisation and identified groundwater types

The hydrogeochemical modelling of the Laxemar subarea is based on data from the cored boreholes KLX01, KLX02, KLX03 and KLX04, in addition to eleven percussion boreholes. The results are presented in Chapter 9 of the L1.2 SDM report /SKB 2006a/; a more detailed description is given in /SKB 2006b/. The overall understanding of the groundwater system at Simpevarp and Laxemar is summarised in Figure 2-5.

The groundwater types A–D in Figure 2-5 are defined as follows:

- **Groundwater type A.** Dilute groundwater, mainly meteoric and Na-HCO_3 in type (< 2,000 mg/L Cl; δ = –11 to –8‰ SMOW). Occurs at depth down to c 500–700 m in Laxemar.
- **Groundwater type B.** Brackish groundwater (2,000–10,000 mg/L Cl; δ = –14 to –11‰ SMOW**)**. Two different types of B water exist:
  - B_L – Laxemar: Meteoric, mainly Na-Ca-Cl in type; glacial/deep saline components.
  - B_S – Simpevarp: Meteoric mainly Na-Ca-Cl in type but some Na-Ca(Mg)-Cl(Br) types (± marine, e.g. Littorina); glacial/deep saline components.
- **Groundwater type C.** Saline (10,000–20,000 mg/L Cl; 18.5–30 g/L TDS; δ = ~ –13 ‰ SMOW (few data)).

  Dominantly Ca-Na-Cl in type at Laxemar increasingly enhanced Br/Cl ratio and SO_4 content with depth at both Simpevarp and Laxemar; Glacial/Deep saline mixtures.

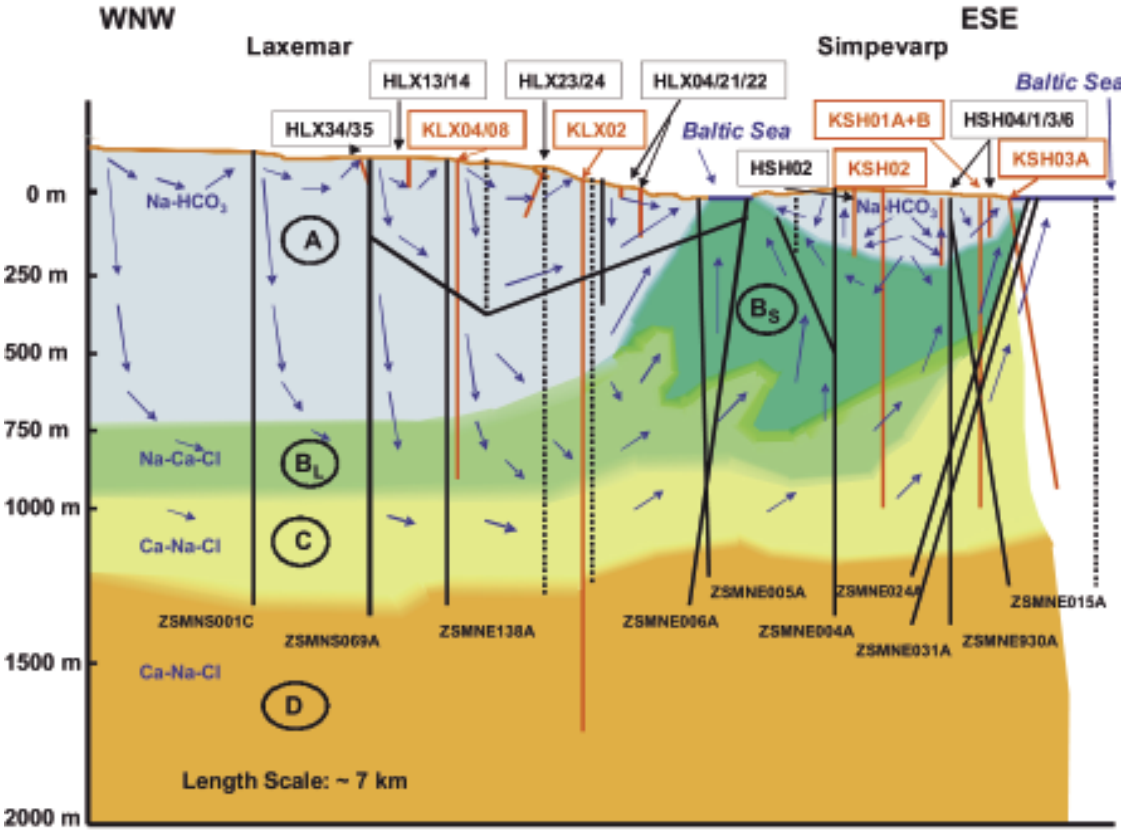

Figure 2-5. *Conceptualisation of the groundwater types identified in a transect from Laxemar to Simpevarp /SKB 2006b/. See text for explanation of groundwater types A–D.*

- **Groundwater type D.** Highly saline (> 20,000 mg/L Cl; to a maximum of ~ 70 g/L TDS; δ = > –10 ‰ SMOW). Only identified at Laxemar (> 1,200 m).

  Dominantly Ca-Na-Cl with higher Br/Cl ratios and a stable isotope composition that deviates from the GMWL when compared to Type C groundwaters; Deep saline/brine mixture.

Compared with the groundwater chemistry of the Simpevarp subarea two major differences can be noted:

A. Fresh to diluted meteoric water dominates down to depth of 500–700 m in Laxemar whereas this groundwater type is only found in the upper 100–200 m in Simpevarp.

B. Brackish to saline water with a marine component has not been identified in the Laxemar subarea.

This means that repository depth at Laxemar represents a mixing zone between fresh diluted water and old saline water usually in-mixed with a glacial component.

Selected water types for laboratory measurements

When the water chemistry for the waters used in the diffusion and batch sorption experiments were selected, the only relevant information from the Laxemar site was the groundwater chemistry from borehole KLX02, showing very dilute water down to at least 800 m. However, additional groundwater samples performed later and included in the Laxemar 1.2 model, show less diluted waters at repository level /SKB 2006b/.

The four water types that have been used in the laboratory measurements of diffusivity and sorption capacity are:

I. Fresh diluted Ca-HCO_3 water; groundwater that can be present in the upper 100–750 m of the bedrock, but also a water type that can be found at larger depths during late phases of glacial periods.

II. Groundwater with marine character, Na-(Ca)-Mg-Cl (5,000 mg/L Cl); a possible transgression of the Baltic Sea may introduce this type of water to repository depth. Assumed to be less important for the Laxemar subarea

III. Groundwater of Na-Ca-Cl type (8,800 mg/L Cl); present groundwater at repository level in the Simpevarp peninsula.

IV. Brine type water of very high salinity, Ca-Na-Cl type water with Cl content of 45,000 mg/L; during a glacial period, brine type waters can be forced to more shallow levels than at present.

The compositions of these groundwater types are specified in Table 2-4.

For the Laxemar samples, water of salinity close to type III above has been used for the diffusivity measurements, however, only the major components (i.e. Ca^{2+}, Na^{+}, Cl^{-} and SO_4^{2-}) were included as the exact ion composition is not expected to influence the diffusion experiments.

For the batch sorption experiments, the groundwater composition is considered to be more important, and three different groundwater compositions have been selected (types I, III and IV). Due to limitations in available amounts of e.g. fracture materials, only two water types have been selected in a smaller set of samples. In these cases, water types I and III have been given priority. However, subsequently analysed waters from KLX03 and KLX04 indicate water with Cl contents around 1,500 ppm at repository depth and additional batch measurements with a groundwater (V) having Cl content in the range of 1,500 to 2,000 ppm is recommended for use in forthcoming measurements.

The composition of the groundwaters used for batch sorption experiments was based on data from KLX02 which was the only available dataset when the measurements started. The subsequently achieved high quality groundwater samples from repository depth in other Laxemar boreholes indicate, however, presence of waters with Cl contents around 1,500 ppm at 500 m depth. Therefore additional batch measurements with a groundwater (V) having Cl content in the range of 1,500 to 2,000 ppm is recommended for use in forthcoming measurements.

Table 2-4. Chemical composition of the groundwater types used in the diffusivity and sorption measurements for the Simpevarp and Laxemar subareas and the Forsmark site; concentrations are given in mg/L.

	Type I (HSH02 0–200 m)	Type II (KFM02A 509–516 m)	Type III (KSH01A 558–565 m)	Type IV (KLX02 1,383–1,392 m)
	Fresh water	Groundwater with marine character	Present ground-water at repository level	Brine type water of very high salinity
Li^+	1.60E–02	5.10E–02	5.80E–01	4.85E+00
Na^+	1.27E+02	2.12E+03	3.23E+03	7.45E+03
K^+	2.16E+00	3.33E+01	1.24E+01	3.26E+01
Rb^+	(2.52E–02)[A]	6.28E–02	4.24E–02	1.78E–01
Cs^+	(1.17E–03)[A]	1.79E–03	1.37E–03	1.86E–02
NH_4^+	(9.47E–02)[A]	4.00E–02	4.00E–02	5.60E–01
Mg^{2+}	1.43E+00	2.32E+02	4.47E+01	1.20E+00
Ca^{2+}	5.21E+00	9.34E+02	2.19E+03	1.48E+04
Sr^{2+}	6.95E–02	7.95E+00	3.23E+01	2.53E+02
Ba^{2+}	(1.29E+00)[A]	1.88E–01	1.88E–01	2.40E–02
Fe^{2+}	(3.64E–01)[C]	1.20E+00	6.86E–01	3.45E+00
Mn^{2+}	2.00E–02	2.12E+00	4.60E–01	1.11E+00
F^-	3.03E+00	9.00E–01	9.67E–01	(1.60E+00)[D]
Cl^-	2.15E+01	5.15E+03	8.80E+03	3.68E+04
Br^-	(2.00E–01)[B]	2.20E+01	7.10E+01	5.09E+02
SO_4^{2-}	8.56E+00	5.10E+02	2.21E+02	1.21E+03
Si(tot)	6.56E+00	5.20E+00	4.70E+00	2.60E+00
HCO_3^-	2.52E+02	1.24E+02	1.20E+01	4.20E+01
S^{2-}	(1.00E–02)[B]	5.00E–02	5.00E–02	5.00E–02
pH	8.58	7.1	7.45	6.8

A) No measurements available, data imported from KSH01 #5263.
B) Based on detection limit.
C) Based on the Fe-tot measurement.
D) No measurements available, data imported from KLX02 #2731.

2.3 Transport data

About 200 rock samples from the boreholes KLX02, KLX03, KLX04, KLX05, KLX06, KLX07 and KLX08 have been selected for the laboratory investigations within the Transport programme hitherto, however there are no data to report from KLX07 and KLX08 yet. The laboratory measurements are performed in order to obtain site-specific diffusion and sorption parameters for the different rock types in the area. The sample selection was made in accordance with /Widestrand et al. 2003/. It primarily includes major rock types, fractures and deformation zones, but also, to a smaller extent, minor rock types and altered bedrock. Measurements are performed on samples from different depths in the boreholes in order to describe the heterogeneity of the retardation parameters and the possible effects of stress release (an issue addressed in the investigation by /Winberg et al. 2003/). The selection of samples from fractures and minor deformation zones was mainly controlled by the indications of water flow, as recorded in flow logs. However, the small amount of material from the fracture coatings and deformation zones has been a limiting factor, which to some extent affected the sampling.

Through-diffusion experiments are performed at Chalmers University of Technology (CTH) in Gothenburg, batch sorption experiments at the Royal Institute of Technology (KTH) in Stockholm and Chalmers University of Technology (CTH). Laboratory electrical resistivity measurements have been performed at GeoVista AB; the results of the resistivity measurements are interpreted in terms of the so-called "formation factor", $F_{m,}$ which can be related to the diffusivity /Johansson 2000, Löfgren 2001/. Porosity measurements and BET surface measurements have been performed at the Swedish National Testing and Research Institute (SP) in connection with the through-diffusion and laboratory resistivity measurements. BET is a method for measuring the specific surface area of a solid material by use of gas adsorption (Brunauer, Emmet, Teller, see /Brunauer et al. 1938/). PMMA (polymethylmethaacrylate) porosity measurement, which is an impregnation method for studying the pore system /Byegård et al. 1998, Hellmuth et al. 1993, 1994/ are performed at the University of Helsinki.

Since the investigations are still in progress, the dataset available for use in the transport modelling is rather limited. The site investigation data available for the L1.2 modelling include data from the water saturation porosity measurements, a small number of through-diffusion data presented in /Börjesson and Gustavsson 2005/, some preliminary batch sorption data and formation factors obtained from laboratory electrical resistivity measurements. Also in situ formation factors, based on interpretations of measurements in the Laxemar boreholes, have been delivered by KTH /Löfgren and Neretnieks 2005/. In addition, some BET surface area data on the major rock types are presented. No results from PMMA (polymethylmethaacrylate) porosity measurements are presented in this model version.

3 Analyses and evaluation of transport data

In this chapter, the data used (i.e. site-specific data and/or data imported from other works) for establishing the retardation models are described. According to the basic conceptual model for radionuclide retention, see Section 1.2.1, the considered retardation processes can be described as:

A. Adsorption on surfaces of materials present in or at the fracture walls, which are considered to be directly accessible (no significant diffusion needed) during the transport. These fracture surface reactions are considered to be independent of the flow rate and the residence time in the fracture, and can thus be simply described by an equilibrium surface sorption coefficient, K_a (m). The retardation obtained by this process can be described by a retardation factor, R_f, defined as:

   $R_f = 1 + \frac{2K_a}{b}$, where b is the aperture of the fracture.

B. Diffusion into the rock matrix and a potential adsorption on the inner surfaces of the rock material. This process is dependent on the following parameters:
   a. The amount of inner volume (pores) in the rock matrix that is available for diffusion, i.e. the porosity, θ_m (–).
   b. The rate at which the radionuclide diffuses in the rock matrix, i.e. the effective diffusivity, D_e (m^2/s).
   c. The partitioning coefficient describing the distribution of the radionuclide between the inner surfaces of the pores and the water volume of the pores, K_d (m^3/kg).

In the time perspective relevant for storage of nuclear waste, the A process can often be neglected compared to the B process.

3.1 Porosity

3.1.1 Methods

Porosity refers to the volume of the rock that is filled with water and available for diffusion. In the conceptual model used in this work, the porosity is considered to be homogeneously distributed in the rock matrix. Any importance of a heterogeneous distribution of porosity in the micro scale can be addressed by PMMA-measurements, e.g. /Hellmuth et al. 1993, 1994/. Such studies are involved in the program for laboratory investigation of transport parameters but they are still in progress and no data are available for this Laxemar 1.2 model.

The porosity data used in the site descriptive transport modelling have mainly been obtained from measurements done on rock samples aimed for diffusion and sorption studies. The method used for determination (SS-EN 1936) consists of a drying step, followed by water saturation of the sample. The drying of the samples is done at a temperature of 70°C, which differs from the temperature (105°C) used in the method (i.e. ISRM 1979) for porosity measurements in the Geology programme of the site investigation. The reason for this is that the samples in the transport programme are designated for other laboratory investigations afterwards. For the interpretation of these laboratory investigations (diffusion and sorption measurements), it is important to avoid the extra chemical and mechanical degradation of the samples that could result from the higher drying temperature.

For a few porosity measurements on samples from KLX02 originating from the work of /Löfgren 2001/ a different porosity method has been used. No elaborate evaluation of possible differences between these methods has yet been done.

It should also be emphasized that a measurement of the porosity is also obtained in the through-diffusion measurements (cf Section 3.2). From the fitting of the experimental results to the diffusion model, the "capacity factor" (denoted α) is obtained, which for the non-sorbing tracer HTO should be equivalent to the porosity. However, the main source of porosity data in this work is the water saturation measurements. Capacity factor measurements are used for comparative purposes only.

3.1.2 Site-specific porosity data

The results of the porosity measurements are summarized in Table 3-1, and are also presented on a detailed sample level in Appendix 1. In the material used, measurements on drill core samples with lengths of 0.5–5 cm are included; however, the majority of the samples with lengths of 3 cm.

Clearly, the large standard deviations of some of the data in Table 3-1, with sample mean minus the uncertainty in some cases in some cases resulting in negative values, indicate that log-normal distributions are more appropriate than, e.g. normal or rectangular distributions for describing the data. Comparisons between the statistics made on all samples and the statistics considering only the samples where alteration and/or fractures were not observed, shows a lower average value for the porosity in the latter case. Furthermore, results for the samples without alteration/fractures also show a lower variability and, consequently, are less likely to display uncertainty ranges with "negative porosity". It is thus obvious that a few number of fractured and altered rock samples have considerable high porosity which causes the large standard deviation for the porosity.

The geological characterisation in binocular microscope shows a great number of small cracks that are 3–15 mm in length and with a width of ≤ 0.5 mm in both fresh and altered rock samples. These cracks are thus larger than intragranular micro cracks /Ståhle 2001/, and cut right through mineral grains. Table 3-1 includes results where the samples with cracks have been excluded; comparisons with the complete datasets indicate that the cracks may increase the porosity. Both concerning the porosity and the diffusivity (cf Section 3.2) of the rock samples, the induced stress release during the sampling is suspected to cause overestimation of the measured parameters.

For the diffusivity, corresponding in situ measurements are available, which enables an evaluation of the effects of the stress release. Since no in situ porosity measurements are available, no direct corresponding address can be made for the porosity parameter. However, porosity and diffusivity are parameters that are generally considered to be closely related to each other, e.g. the Archies law, /Parkhomenko 1967/, cf Section 3.2.3. Based on this consideration, estimations of the impact of stress release on the porosity measurements could be obtained from the in situ diffusivity measurements.

Another possible effect of the sampling of the rock is that the drilling and sawing may induce increased numbers of micro-fractures in the samples, which thus may increase the porosity in the rock closest to the edges of the sampled rock. It follows that this effect should be more pronounced in shorter rock samples. However, a limited, length dependent connectivity of the porosity would result in decreased apparent porosity with increased sample length. The effect of the sample length is illustrated in Table 3-2, which indicates

that the measurement method gives an increase in porosity values with shorter sample lengths. This statement is supported by earlier porosity measurements in connection with diffusion experiments /Johansson et al. 1997/. It should be noted, however, that the statistical significance of the data in Table 3-2 is questionable (few samples), which is also the case for some of the results in Table 3-1.

In summary, it is indicated that the variations between porosity results obtained using different size of the rock samples are more significant than the variations in the results of the different rock types used. Taking the uncertainty within the different rock types into consideration, the differences in most cases is overlapped by the uncertainty.

Alteration of the rock is suspected to be a factor that can influence the porosity, as have been shown in previous investigations /Eliasson 1993/. In this stage of the laboratory investigations, there is not enough data to quantify an alteration effect on the porosity, but this effect should be considered in forthcoming evaluations of data from the on-going site investigations.

It should also be noted that the porosity values for Ävrö granite and quartz monzodiorite in the geological L1.2 model /SKB 2006a, Chapter 11/ are higher than those presented in Table 3-1. This could be due to that the results presented by the Geology programme are from mainly from outcrops and not from drill cores.

Table 3-1. Porosities (vol-%) of different rock types from the Laxemar area (number of samples within parenthesis). Drill core samples with lengths of 0.5–5 cm have been used, however, with the vast majority of the samples having lengths of 3 cm. The values are given as mean value ± 1σ of the experimental dataset (non-log and log_{10} values for each rock type).

Rock type	All rock samples (n)	Rock samples without alteration and/or cracks (n)
Ävrö granite	0.32±0.19 (143) $10^{-0.55\pm0.20}$	0.27±0.09 (112) $10^{-0.59\pm0.16}$
Quartz monzodiorite	0.26±0.26 (22) $10^{-0.72\pm0.33}$	0.17±0.08 (15) $10^{-0.82\pm0.23}$
Fine-grained dioritoid	0.32±0.53 (7) $10^{-0.88\pm0.56}$	0.14±0.14 (5) $10^{-0.98\pm0.35}$
Fine-grained diorite-gabbro	0.22±0.08 (7) $10^{-0.68\pm0.14}$	No samples excluded
Fine-grained granite	0.24±0.03 (5) $10^{-0.62\pm0.05}$	0.22±0.0002 (3 $10^{-0.66\pm0.0004}$
Granite	0.61±0.33 (2) $10^{-0.25\pm0.25}$	0.38 (1) $10^{-0.42}$

Table 3-2. Porosities (vol-%) for rock samples of different lengths sampled at the same position (number of samples within parenthesis). The values are given as mean value ± 1σ of the experimental dataset.

	Samples 0.5 cm (3)	Samples 1 cm (3)	Samples 3 cm (3)	Samples 5 cm (3)
Ävrö granite KLX02A 216.69–217.00 m	0.41±0.05	0.28±0.05	0.18±0.04	0.17±0.02
Quartz monzodiorite KLX04, 489.48–489.83 m	0.25±0.06	0.23±0.08	0.11±0.04	0.11±0.07

3.2 Diffusion

3.2.1 Methods and parameters

In this work, the term diffusion refers to the process of the exchange of a tracer diffuses between the fracture water volume and the micro fractures of the rock matrix. Thereby, an interaction can occur in which the inner surfaces of the rock matrix become available for sorption, and the tracers can be significantly retarded in their transport. The present work addresses diffusion processes in the aqueous phase only; potential diffusive mobility in the adsorbed state (so-called surface diffusion /Ohlsson and Neretnieks 1997/) is not considered.

Two main methods for the determination of the diffusivity of the rock materials are used within the SKB site investigations /Widestrand et al. 2003/:

- Through-diffusion measurements; a method where the effective diffusivity, D_e (m^2/s), is determined by studying the diffusion rate of tritiated water (HTO) through a rock sample (HTO is used in the site investigations; the method can be applied also with other tracer solutions).
- Resistivity measurements; a method where the information on the diffusivity is obtained from the in situ resistivity measurements of naturally electrolyte-saturated rock samples.

The diffusion process is quantified in terms of the formation factor, F_m (–). This parameter quantifies the reduced diffusion rate obtained in the rock material relative to the diffusion rate in pure electrolyte. It is thus calculated from the results of the through-diffusion studies, as:

$$F_m = \frac{D_e}{D_w} \qquad (3\text{-}1)$$

where D_w (m^2/s) is the diffusivity of tritiated water in pure water, i.e. 2.13×10^{-9} m^2/s /Li and Gregory 1974/.

For the resistivity measurements, F_m is the parameter produced by the method, i.e. the ratio of the resistivity of a given electrolyte to the resistivity of the rock sample with the pores saturated with the same electrolyte.

The resistivity can be measured both in laboratory experiments (where the rock samples are saturated with 1 M NaCl) and in borehole in situ experiments. For obvious reasons, no saturation of the rock matrix with a known electrolyte can be done in in-situ experiments. In this case, the composition of the pore liquid must be estimated based on hydrogeochemical sampling and analysis, commonly assuming the same composition in the matrix as in the groundwater in neighbouring fractures. A further complication is that a lower salinity than 1 M NaCl, which thus likely could be present in the pores in in situ rock, according to /Ohlsson and Neretnieks 1997/ attributes a significant part of the conductivity to the surface ion mobility.

3.2.2 Through-diffusion studies

Site-specific data

Site specific rock materials from the Laxemar site have been sampled and used in through-diffusion measurements in accordance with the SKB method description MD 540.001 (SKB internal document). These measurements are time consuming, and steady state conditions (necessary for final evaluation) have not been obtained in most samples.

For the parameterisation of the L1.2 retardation model, results for only two sets of samples are presented in which steady state has been obtained. However, preliminary results from a larger number of samples, where steady state has not been obtained, are included for comparative purposes.

The diffusivity is determined by studying the diffusion of tritiated water (HTO) through a slice of rock. A slice of water-saturated rock is mounted in a diffusion cell, where the start cell is filled with water spiked with HTO tracer and the other side is filled with non-spiked water. The rate of diffusion is evaluated from the rate of the in-growth of the HTO tracer in the originally non-spiked water volume. The effective diffusivity, D_e (m^2/s), and the rock capacity factor, α (–), are calculated by fitting the model equation /Crank 1975/:

$$C_r = \frac{C_2 V_2}{C_1 A} = \frac{D_e t}{l^2} - \frac{\alpha}{6} - \frac{2\alpha}{\pi^2} \sum_{n=1}^{\infty} \frac{(-1)^n}{n^2} \exp\left\{ - \frac{D_e n^2 \pi^2 t}{l^2 \alpha} \right\} \qquad (3\text{-}2)$$

where C_2 (Bq/m^3) is the accumulated tracer concentration in the target cell at the time t (s), V_2 (m^3) is the volume of the target cell, C_1 (Bq/m^3) is the tracer concentration in the start cell, A (m^2) is the geometric surface area of the rock sample, and l (m) is the length of the rock sample. Provided that the tracer used is non-sorbing, the rock capacity factor α (–) should be equal to the porosity measured with, e.g. water saturation technique.

The results from the evaluation of the finished and on-going through diffusion experiments are presented in Table 3-3 and examples of through diffusion breakthrough curves are given in Figure 3-1. For the 1 cm samples, a general experimental problem is observed when obtaining a contamination of tracer already in the start of the experiment. This complicates the evaluation, especially for the rock capacity factor, α (–), which more or less is obtained from the straight line intercept with the x-axis.

As mentioned above, only two series of the Laxemar samples have been considered to have reached a steady state. The first is a series consisting of three 10 mm thick samples of Ävrö granite. They give formation factors in the range of (5.2–7.5)E-5, i.e. slightly lower than the values obtained for the corresponding laboratory resistivity measurements but rather similar to the values obtained for the resistivity measurements performed in situ (cf Section 3.2.3). The other series consists of three 30 mm samples of coarse grained Ävrö granite, for which ~ 5 times higher formation factors are obtained compared to the more fine-grained samples mentioned earlier. This is not at all unexpected; the presence of larger grains is suspected to cause larger voids between the grains and therefore also less diffusion resistance.

The preliminary results from the samples where steady state has not been obtained are also given in Table 3-3. These preliminary results indicate a general consistency with the laboratory resistivity measurements, possibly with the through diffusion results giving somewhat lower formation factors than laboratory resistivity measurements.

Comparisons between the rock capacity factor and the porosity determined by water saturation technique is restricted to KLX02A 235.0–235.1 m samples. For these samples, it is indicated a factor of ~ 3 higher capacity factors compared to the measured porosities. At this stage, no elaborate analysis for the reason of the difference has been made. If this difference can be established when a larger number of comparisons have been made (e.g. in forthcoming versions of the retardation model), this may call for a closer consideration and/or investigation.

Table 3-3. Preliminary results from through-diffusion experiments on rock samples from KLX02A and KLX04A. The effective diffusivity, D_e, and the rock capacity factor, α, were obtained from least-square fits to the experimental data.

Rock type	SKB ID	Sample length (mm)	D_e (m^2/s)	F_m (through diffusion)	F_m (electr. resistivity)[A]	α (–)[B]	Water sat. porosity (vol%)
Steady state considered to have been obtained							
Ävrö granite	KLX02A 216.70–216.71	10	1.1E–13	5.2E–5	Laboratory: (1.4±1.0)E–4	–[C]	0.23
	KLX02A 216.80–216.81	10	1.3E–13	6.1E–5		–[C]	0.21
	KLX02A 216.91–216.92	10	1.6E–13	7.5E–5	In situ (6.2±2.9)E–5	–[C]	0.33
Ävrö granite, coarse grained	KLX02A 235.02–235.05 m	30	6.5E–13	3.1E–4		1.0E–2	0.36
	KLX02A 235.05–235.08 m	30	6.1E–13	2.9E–4		1.0E–2	0.39
	KLX02A 235.08–235.11 m	30	6.8E–13	3.2E–4		1.4E–2	0.39
Steady state not considered to have been obtained							
Ävrö granite	KLX02A 216.71–216.74	30	4.9E–14	2.3E–5	Laboratory: (1.4±1.0)E–4	1.6E–3	0.13
	KLX02A 216.81–216.84	30	5.5E–14	2.6E–5		1.9E–3	0.19
	KLX02A 216.92–216.95	30	7.5E–14	3.5E–5	In situ (6.2±2.9)E–5	2.5E–3	0.21
	KLX02A 216.74–216.79	50	2.9E–14	1.4E–5		5E–4	0.15
	KLX02A 216.84–216.89	50	3.2E–14	1.5E–5		5E–4	0.16
	KLX02A 216.95–217.00	50	3.3E–14	1.5E–5		6E–4	0.19
	KLX02A 258.96–258.99	30	9.8E–14	4.6E–5		3.1E–3	0.23
	KLX02A 440.21–440.24	30	1.6E–14	7.5E–6		4E–4	0.15
	KLX02A 600.19–600.22	30	1.2E–13	5.6E–5		6.4E–3	0.27
(Fract., altered)	KLX04A 920.40–920.43	30	4.1E13	1.9E–4		1.2E–2	0.80
Quartz monzo-diorite	KLX04A 489.50–489.53	30	1.1E–13	5.2E–5	Laboratory: (3.6±3.5)E–5	–[C]	0.09
	KLX04A 489.62–489.65	30	6.5E–14	3.1E–5		–[C]	0.15
	KLX04A 489.75–489.78	30	1.2E–14	5.6E–6	In situ: (2.1±0.1)E–5	–[C]	0.10
	KLX04A 489.53–489.58	50	1.4E–13	6.6E–5		–[C]	0.19
	KLX04A 489.65–489.70	50	1.7E–14	8.0E–6		–[C]	0.05
	KLX04A 499.70–499.73	30	4.8E–14	2.3E–5		–[C]	0.10
Fine-grained dioritoid	KLX02A 682.34–682.37	30	1.2E–14	5.6E–6	Laboratory: 9.2E–6	3E–4	0.06
	KLX02A 682.37–682.40	30	1.2E–14	5.6E–6		3E–4	0.06
	KLX02A 682.40–682.43	30	1.2E–14	5.6E–6	In situ: –	3E–4	0.12
	KLX02A 700.15–700.18	30	1.5E–14	7.0E–6		4E–4	1.49
	KLX04A 277.66–277.69	30	2.3E–14	1.1E–5		3E–4	0.39
Fine-grained diorite gabbro	KLX02A 387.78–387.81	30	2.0E–13	9.4E–5	Laboratory: (6.4±4.2)E–5 In situ: (3.4±1.7)E–5	4.2E–3	0.36
Fine-grained granite	KLX04A 719.38–719.41	30	2.8E–14	1.3E–5	–	–[C]	0.26

A) Average value for all measured samples from Laxemar, cf Table 3-4.
B) For comparison with the numerical values of water saturation porosity (given as %), the values should be multiplied with 100.
C) A small contamination in the target cell already at an early stage of the experiment made it impossible to evaluate the formation factor. Instead, the measured water saturation porosity was applied in the evaluation, i.e. only the diffusivity was estimated.

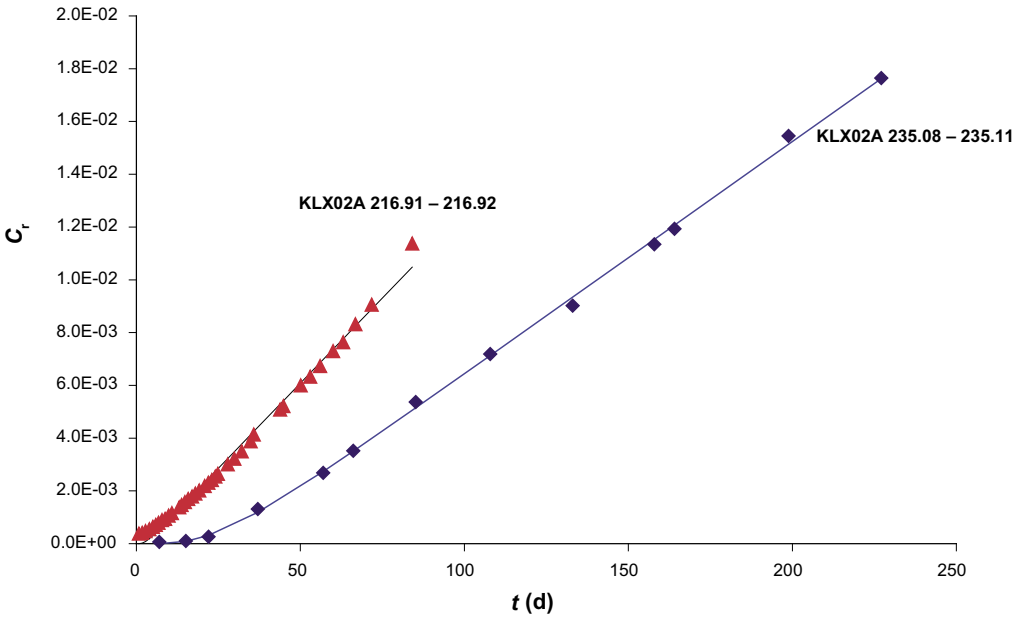

Figure 3-1. *Examples of breakthrough curves for the through-diffusion experiments. Results are presented for a 10 mm sample from KLX02A 216.91– 216.92 m and a 30 mm sample from KLX02A 235.08–235.11 m. The former is a sample of Ävrö granite of average grain size, while the latter sample is a pronounced coarse grained Ävrö granite.*

3.2.3 Electrical resistivity

A summary of the results of the electrical resistivity measurements reported by /Löfgren and Neretnieks 2005, Löfgren 2001, Thunehed 2005ab/ is provided in Table 3-4; the individual measurement results can be found in Appendix 2. In Table 3-4, the results are expressed in terms of both non-log and log10 values. Similar to the porosity data discussed above, standard deviations in the non-log values are in many cases of the same order as, or even larger than, the mean values. Some general observations made in the electrical resistivity data are presented in the following.

In Table 3-4, no comparisons are made of the formation factors determined by electrical resistivity measurements to the formation factors determined by through diffusion experiments, cf Section 3.2.2. The reason for omitting such a comparison in this report is that only two series of through-diffusion measurements are presently available for Laxemar rock types where a steady state has been obtained, cf Table 3-3. These two series consist of one series of coarse grained Ävrö granite and one series of 10 mm long samples of Ävrö granite. These samples are, as described in Section 3.2.2, suspected to give an overrepresentation higher formation factors. A general comparison of these two techniques therefore has to be postponed until later versions of the retardation model where a larger number of formation factors obtained by through-diffusion experiments is expected to be available.

Laboratory resistivity versus porosity

As expected, a tendency of increased formation factor with increasing porosity can be observed in the results (Figure 3-2). A quite interesting fact is observed in the presentation of the data in log-log scale (Figure 3-3) where a representation of the so-called Archie's law, (F_m=0.71*$\theta_m^{1.58}$), /Parkhomenko 1967/ indicate a general agreement with the obtained results.

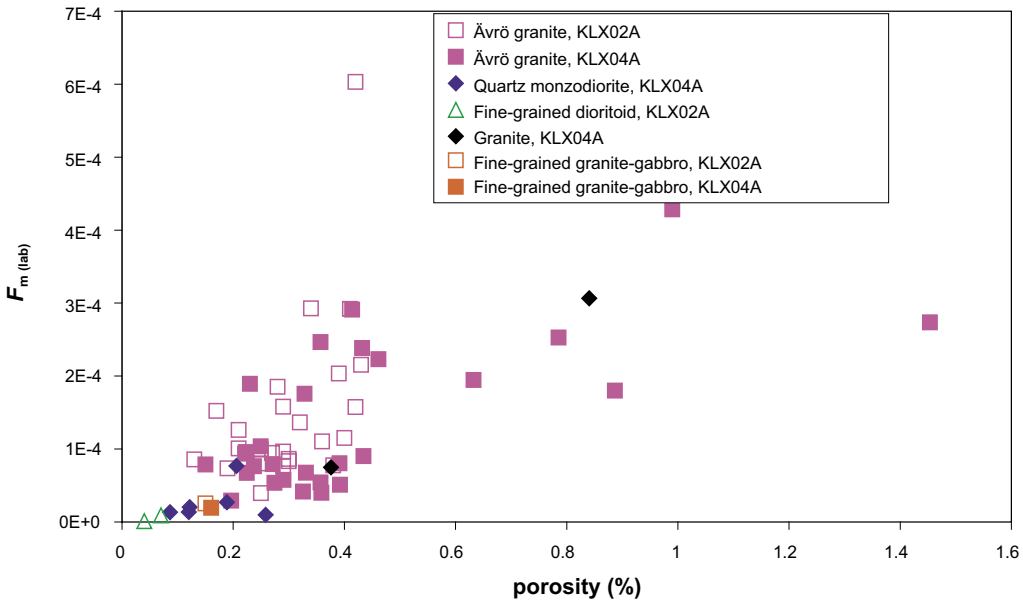

Figure 3-2. *Formation factor versus the porosity, using formation factors determined in electrical resistivity measurements in the laboratory /Löfgren and Neretnieks 2005/. The porosities were measured using the water saturation method (SS-EN 1936).*

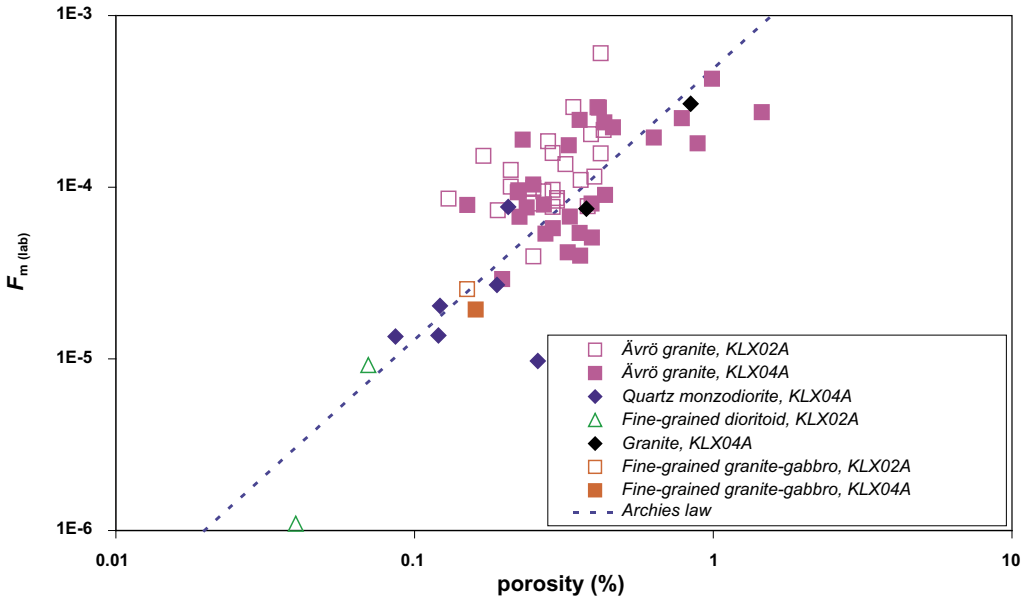

Figure 3-3. *Formation factor versus the porosity (in log-log scale), using formation factors determined from electrical resistivity measurements in the laboratory /Löfgren and Neretnieks 2005/. The porosities were measured using the water saturation method (SS-EN 1936). A representation of Archie's law (F_m=0.71*$\theta_m^{1.58}$) is included for comparison.*

Formation factor versus borehole length

Data are presented both for the laboratory measurements (Figure 3-4) and for the in situ measurements (Figure 3-5). The very large number of measurements in the interval 350–400 m in KLX02 originates from the very careful investigation by /Löfgren 2001/. A comparison indicates that the values obtained for the in situ measurements are lower than the corresponding values obtained for the laboratory measurements. This is illustrated in Figure 3-6 where the ratio of in situ and laboratory measurements is given as a function of the borehole depth. The ratio is generally below 1 but some exceptions to this exist.

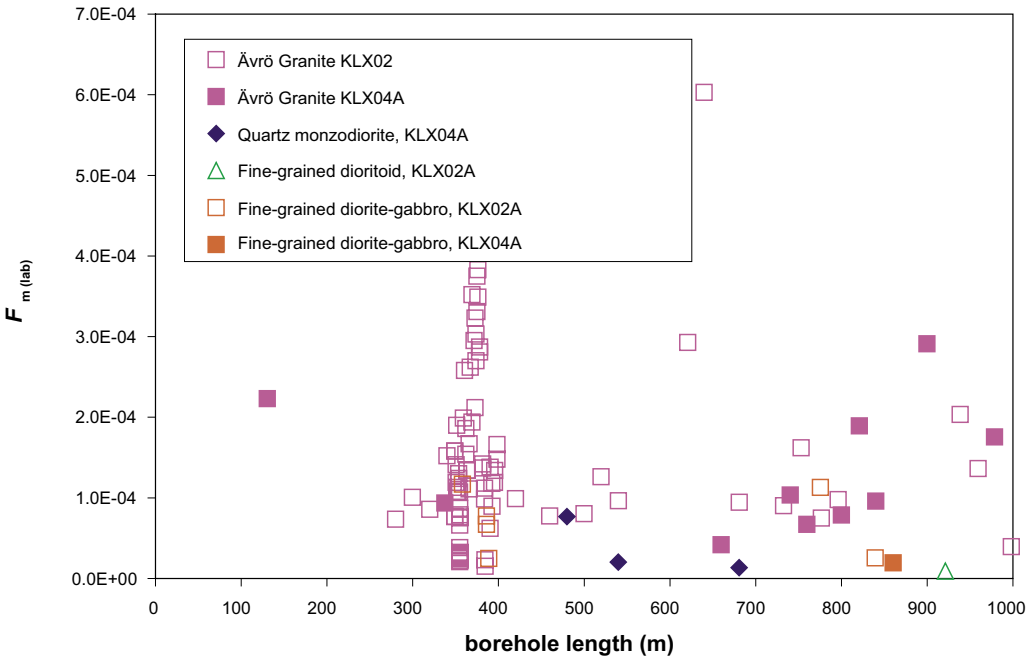

Figure 3-4. *Formation factors measured with electrical resistivity in the laboratory versus the borehole length, i.e. the position in the borehole where the sample has been taken.*

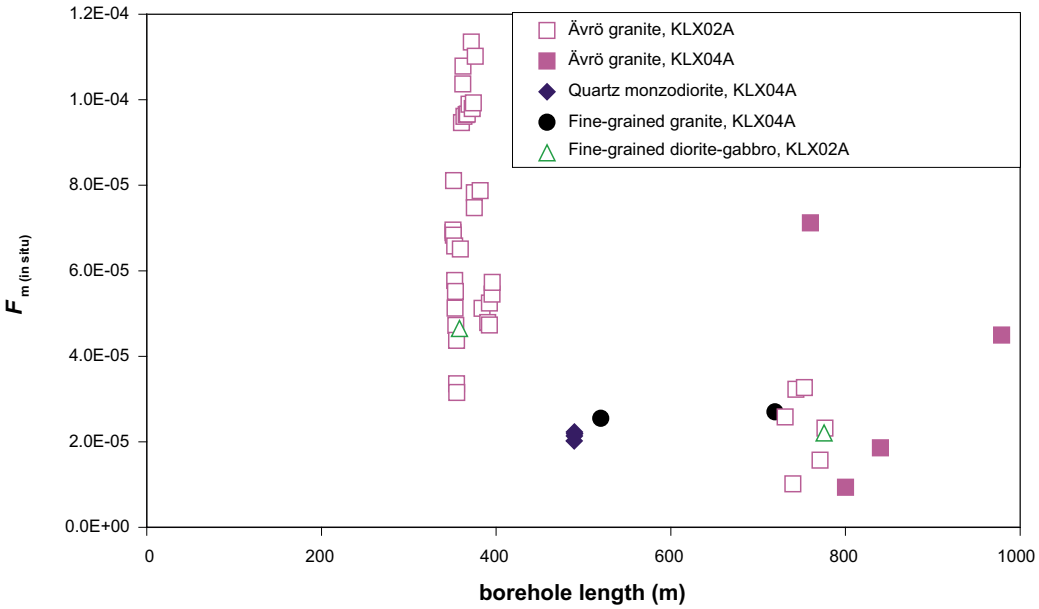

Figure 3-5. *Formation factors measured with electrical resistivity in situ versus the borehole length.*

However, due to large scatter in the dataset, it is difficult to identify any particular trend in the laboratory data. For example, no clear trend can be observed that indicates a significant increase in diffusivity in samples from larger depths, which, if present, could indicate an increased effect of stress release on these samples (cf Figure 3-6). It is also difficult to observe such a trend in the representation of the porosity versus the sample depth for the laboratory samples (Figure 3-7).

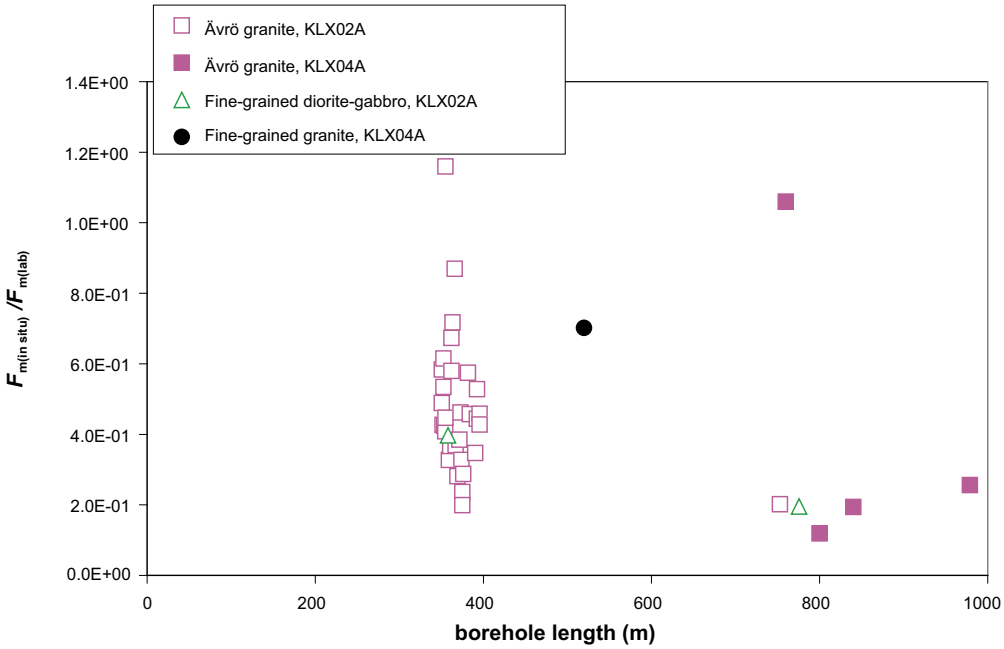

Figure 3-6. *Ratio of the formation factors measured in the laboratory and in situ with electrical resistivity versus the borehole length. The marked area in the upper right part of the figure corresponds to a number of samples at large depth that are suspected to have undergone a marked stress release, i.e. the F_{lab} is significantly larger than the corresponding $F_{in\ situ}$.*

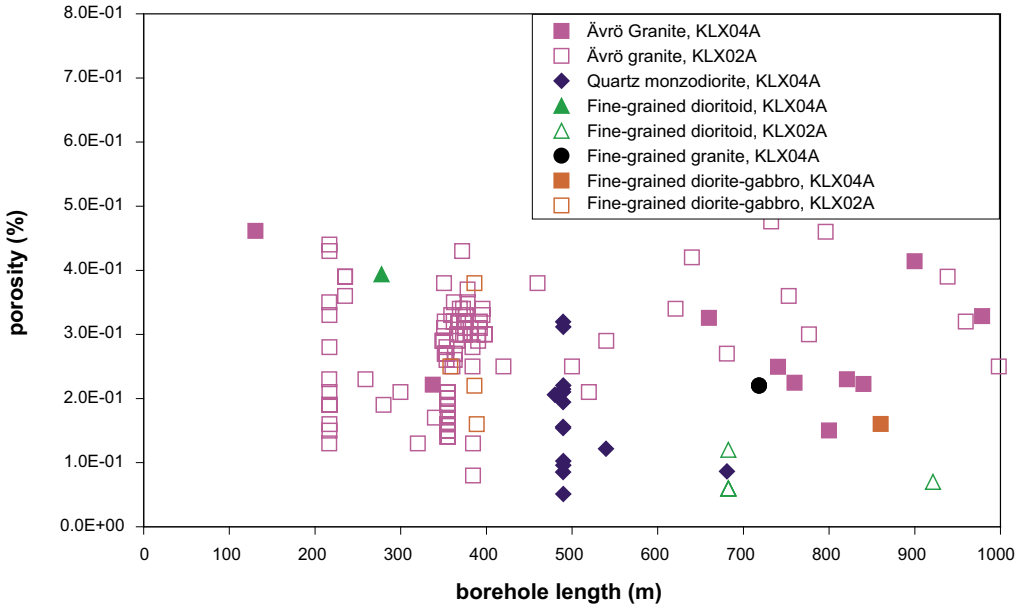

Figure 3-7. *Porosity, measured in the laboratory using the water saturation method, versus the borehole length.*

Linear and logarithmic distribution of formation factor and porosity

For the rather larger amount of data available for the rock type Ävrö granite, representations in linear and logarithmic scales of the formation factor (Figure 3-8 and 3-9) and the porosity (Figure 3-10 and 3-11) are presented. The results give some indications that the log-normal distribution is a better model for interpretation of the results. Furthermore, an additional and obvious advantage of using log-normal distributions is the possibility of avoiding uncertainty intervals that go into the negative area.

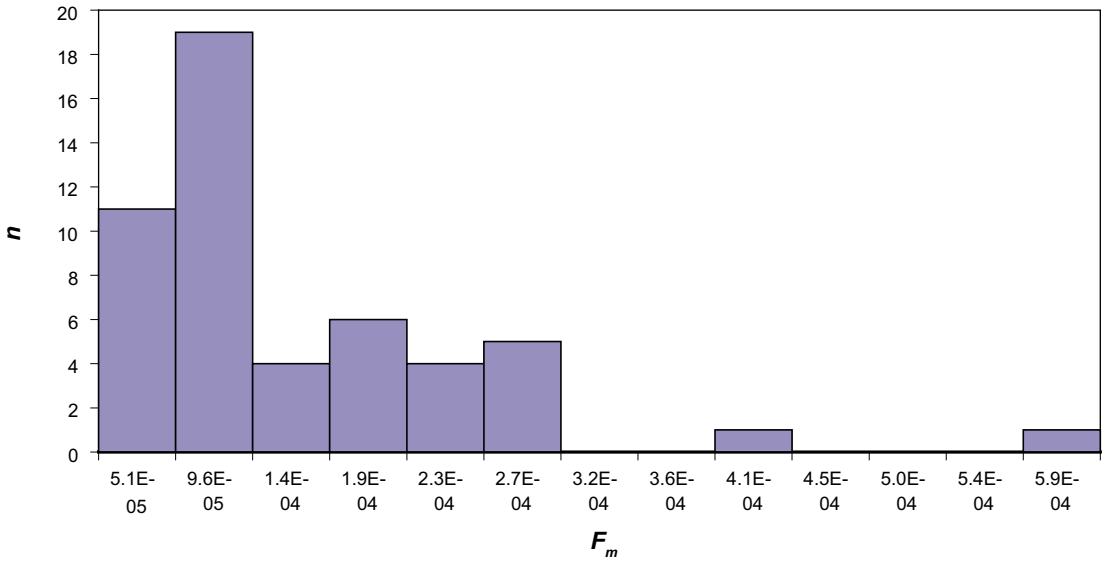

Figure 3-8. *Distribution of the formation factor in lin-scale for the Ävrö granite samples.*

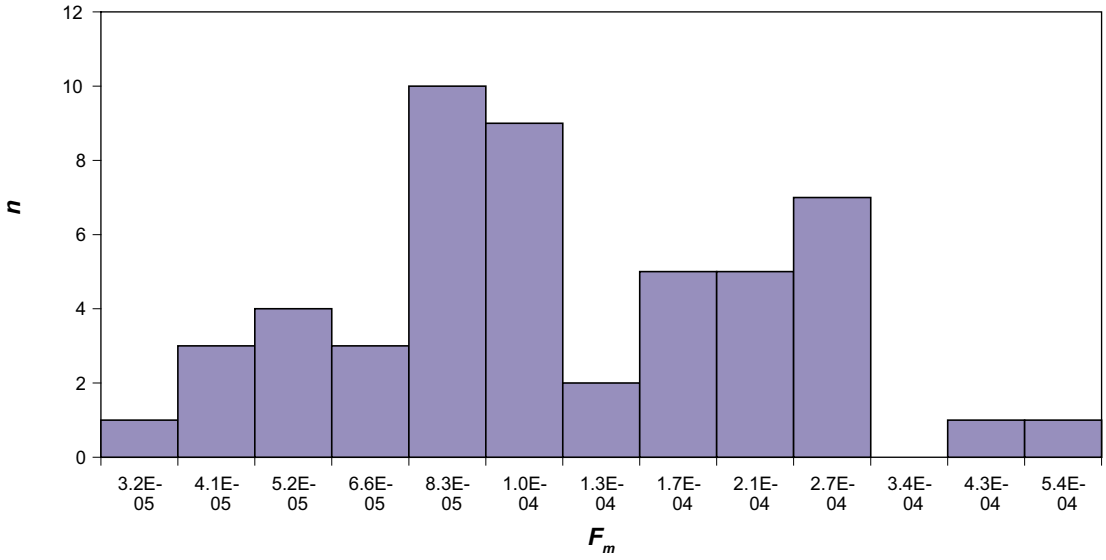

Figure 3-9. *Distribution of the formation factor in log-scale for the Ävrö granite samples.*

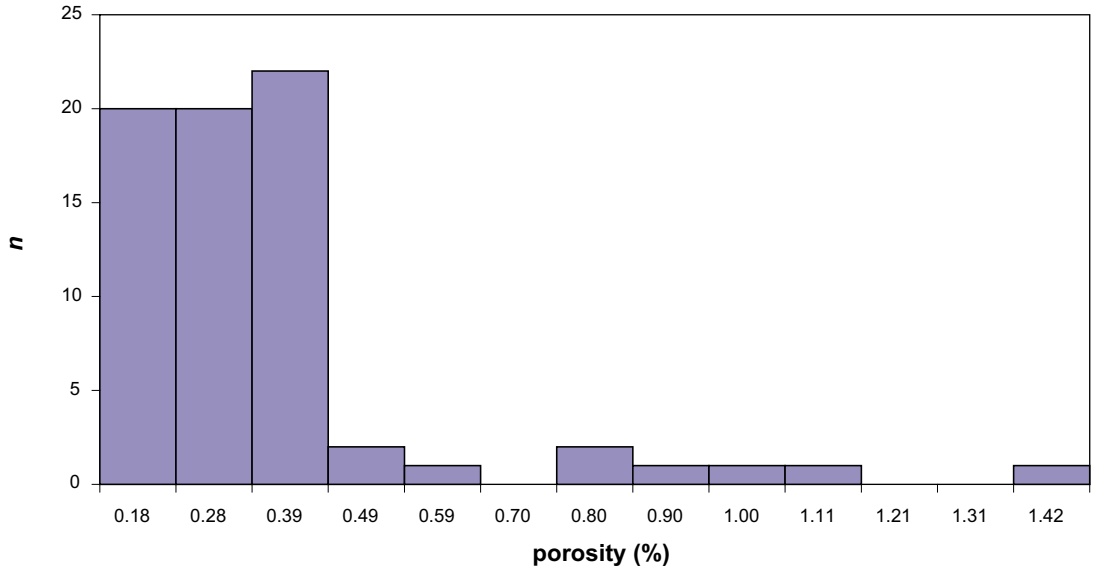

Figure 3-10. *Distribution of porosity in lin-scale for the Ävrö granite samples.*

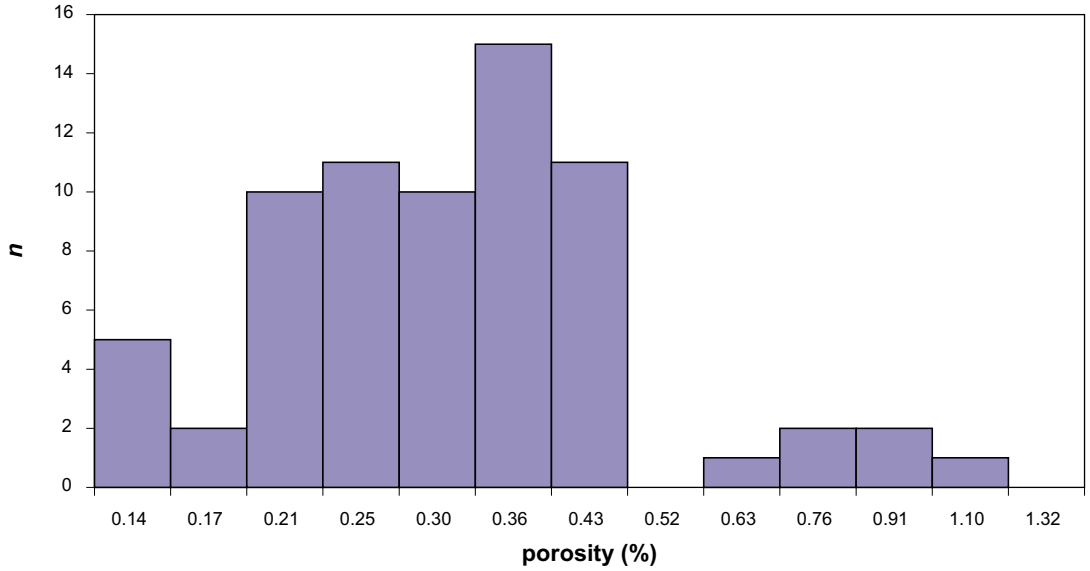

Figure 3-11. *Distribution of porosity in log-scale for the Ävrö granite samples.*

Table 3-4. Summary of formation factors for the Laxemar rock types determined with electrical resistivity measurements. Only samples without presence of visible (binocular inspection) microfractures and alteration have been included. The values are given as mean values ± one standard deviation of the considered datasets (non-log and log_{10} values). The numbers of values upon which the statistics are based are given within brackets.

Method	Quartz monzodiorite	Ävrö granite	Fine-grained dioritoid	Fine-grained diorite-gabbro	Granite
Electrical resistivity, lab	(3.6±3.5)E–5 [3] $10^{-4.56\pm0.39}$	(1.4±1.0)E–4 [114] $10^{-3.98\pm0.35}$	9.2E–6 [1] $10^{-5.04}$	(6.4±4.2)E–5 [7] $10^{-4.30\pm0.33}$	7.5E–5 [1] $10^{-4.13}$
Electrical resistivity, in situ	(2.14±0.09)E–5 [6] $10^{-4.67\pm0.02}$	(6.2±2.9)E–5 [43] $10^{-4.27\pm0.27}$		(3.4±1.7)E–5 [2] $10^{-4.49\pm0.22}$	

3.3 Sorption

3.3.1 BET surface area

Since the adsorption of radionuclides is taking place on the surfaces of the rock material, the quantification of available surface areas is an important estimation of the sorption capacity of the rock material. For example, different ferric oxides have significant surface areas and have been shown to be highly adsorbing minerals for cations that adsorb with surface complexation, see, e.g. /Jakobsson 1999/. Furthermore, presence of clay minerals (as a group identified as a significant potential sink for Cs^+) will also cause increased surface areas in the measurements on rock samples.

Although at this stage no method is available for establishing a quantitative relationship between specific surface areas and sorption parameters, results of BET surface area measurements /Brunauer et al. 1938/ are included in the retardation model as qualitative data important for the understanding of the sorption processes. BET measurements have been performed on site-specific materials according to the ISO 9277 standard method. The results of the measurements on the Laxemar site rock types are given in Table 3-5 and Table 3-6.

Table 3-5. Measured BET surface area for the fractions 0.063–0.125 mm and 2–4 mm of crushed and sieved matrix rock samples. Measured results are presented together with the results of an extrapolation of the results in order to obtain an inner surface area (concept equivalent to the concept in the K_d extrapolation, cf Equation 3-3).

Rock Type	Borehole	Depth	BET surface area 0.063–0.125 mm (m^2/g)		BET surface area 2–4 mm (m^2/g)		Extrapolated inner BET surface area (m^2/g)
			min	max	min	max	
Ävrö granite	KLX02A	217.00–217.20	0.3985	0.4016	0.0569	0.0655	0.050±003
		235.11–235.31	0.2687	0.2919	0.0437	0.0451	0.036±0.008
		359.83–360.03	0.2938	0.3407	0.0452	0.0504	0.039±0.017
		509.50–509.70	0.2441	0.2641	0.0252	0.0333	0.022±0.008
		540.42–540.62	0.5406	0.5771	0.0439	0.0457	0.028±0.013
		753.80–754.00	0.4322	0.4402	0.0352	0.0489	0.029±0.006
		(936.11–936.37)[A]	0.5803	0.6153	0.0927	0.0984	0.079±0.013
	KLX03A	522.61–523.00	0.2196	0.2809	0.035	0.0356	0.028±0.022
	KLX04A	464.62–465.07	0.291	0.3501	0.0181	0.0259	< 0.03
	KLX05A	461.77–462.17	0.2505	0.3627	0.0361	0.0552	< 0.07
						Average	0.032±0.020
Fine-grained dioritoid	KLX02A	682.70–682.90	0.3501	0.366	0.0322	0.0425	0.027±0.007
		805.05–805.23	0.8058	0.845	0.1012	0.1016	0.078±0.014
	KLX05A	428.57–428.97	0.9137	0.9281	0.0759	0.1095	0.066±0.013
						Average	0.057±0.027
Quartz monzodiorite	KLX03A	635.56–635.96	0.3088	0.3159	0.0151	0.0274	0.012±0.005
	KLX04A	489.85–490.25	0.3412	0.4348	0.0404	0.0431	< 0.06
		724.26–724.72	0.6453	0.6641	0.0155	0.0162	< 0.007
	KLX05A	482.30–482.70	0.8724	0.9056	0.0889	0.0982	0.068±0.013
		605.90–606.31	0.4162	0.5158	0.0124	0.025	< 0.04
		921.52–921.93	0.3247	0.3367	0.0237	0.0328	0.018±0.005
						Average	< 0.05
Fine-grained diorite-gabbro	KLX02A	387.53–387.73	0.7688	0.8004	0.072	0.0869	0.057±0.013
Diorite-Gabbro	KLX05A	364.14–364.54	0.483	0.4907	0.0472	0.0585	0.039±0.005

A) Altered rock, therefore treated separately and not included in the average

Table 3-6. Measured BET surface area for the rock material sampled in close vicinity of fractures (non-crushed, unless otherwise stated). Measured results for different size fractions are presented together with the results of an extrapolation of the results in order to obtain an inner surface area (concept equivalent to the concept in the K_d extrapolation, cf Equation 3-3 below).

Rock type/ Fracture type or Structure element type	Sampling position Borehole depth (m)	Sample description	BET surface area < 0.125 mmA (m^2/g)		BET surface area 2–4 mm (m^2/g)		Extrapolated inner BET surface area (m^2/g)
			min	max	min	max	
Altered Ävrö granite/ Facture type D	KLX03A 278.27	Fracture filling, extracted by scraping	23.5B	24.8B			
Ävrö granite/ Structure element type 1(4)	KLX04A 874.48–874.64	Material extracted by scraping from fracture rim zone material	24.5	25.2			
Ävrö granite/ Structure element type C	KLX04A 951.3–951.44	Sampled loose fracture filling material	7.2313	7.2829	3.0477	3.6976	3.25±0.24
Fine-grained diorite-gabbro/ Structure element type 2	KLX03A 732.62	Sampled loose fracture filling material	7.88	7.89			
Fine-grained diorite-gabbro, Fracture type B	KLX03A 736.96–737.23	Fracture filling material, extracted by scraping	2.63	2.74			
Fine-grained diorite-gabbro, Structure element type 1	KLX06A 384.00–384.04	Gouge material, crushed and sieved	24.0593	24.1907	9.7944C		9.3±0.1

A) Size fraction 0–0.125 mm unless other notification.
B) 0.063–0.125 mm size fraction used.
C) Only a single sample measured.

The results of the BET measurements indicate that the crushing of the rock material causes formation of new surfaces that are non-representative for the intact rock. From the results of the samples from major rock types, one can estimate that the 0.063–0.125 mm fraction shows 5–50 times higher BET surface than the corresponding 2–4 mm size fraction. Using the results for an extrapolation to obtain an inner BET surface (a concept equivalent to the interpretation of sorption results, cf Section 3.3.2 and Equation 3-3) values are obtained in the range of 0.018–0.079 m^2/g. These values are consistent with the results for experimental investigation of the BET surface of intact rock (e.g. Neretnieks, unpublished data, personal comm, who found a BET surface of 0.025 m^2/g for a 18 mm thick fine-grained granite from Äspö).

An implication of the results of the BET surface measurements is that the consideration that the batch sorption experiments with crushed rock material for the determination of sorption coefficients will be determined on rock samples where < 90% of the surfaces involved should be considered as non-representative for intact rock. Although the concept applied for evaluation of the sorption coefficient (cf Equation 3-3 in Section 3.3.2) is aimed to compensate for this, a general doubt could be raised whether the results batch sorption determined sorption coefficients really is done on material fully representative for intact rock. This is an issue that should be further addressed in forthcoming version of site descriptions, when site specific sorption data are available.

An interesting observation is that material carefully sampled from natural fractures (results in Table 3-6) shows significantly higher BET surface compared to the crushed major rock types. A possible explanation for this trend is the presence of e.g. clay material and ferric oxides close to the fractures, i.e. materials that in different alteration processes have become very porous and thereby turned into "large surface-area" materials. Since differences of a factor 100–1,000 compared to the estimated inner BET surfaces of the non-altered major rock types are observed, it is obvious that fracture materials can provide an important sinks for dispersed radionuclides. This is probably most valid for radionuclides with sorption characteristics dominated by surface complexation.

3.3.2 Sorption data

The process "sorption" is here defined as the adsorptive interaction of radionuclides with the surfaces of the rock material. In the somewhat simplified approach taken in this work, sorption is considered to be:

- Linear (i.e. no concentration effect on the sorption).
- Fast and reversible compared to the considered time perspective (no chemical kinetic effects are addressed for the sorption processes).

The concept used for the sorption processes is the same as described in the "laboratory strategy report" /Widestrand et al. 2003/. This means that the source of sorption data is batch laboratory experiments performed using crushed and sieved rock material. The results from the measured distribution of tracer between the rock and water phase will be interpreted as:

- Adsorption of the tracers on the outer surfaces of the rock material, determined by the surface sorption parameter, K_a (m).
- Adsorption of the tracers on the inner surfaces of the rock material, determined by the volumetric sorption parameter, K_d (m^3/kg).

In the considered transport concept, the K_a parameter is used only to estimate the minor part of tracer retention that takes place via the sorption on the fracture walls, and is thus of less importance for long time perspectives. The major part of the retention is considered to be caused by the diffusion of the radionuclides into the rock matrix and the subsequent sorption on the inner surfaces of the rock material.

The evaluation of the batch sorption experimental results to sorption parameters is done according to:

$$R_d = K_d + \frac{6K_a}{d_p \rho} \qquad (3\text{-}3)$$

where R_d (m^3/kg) is the measured tracer distribution between solid and liquid phases, d_p (m) is the average particle diameter, and ρ (kg/m^3) is the rock density. A graph of R_d versus $1/d_p$ gives an intercept corresponding to the K_d value, and a slope corresponding to $6K_a/\rho$. This concept of evaluation implies the following assumptions:

- The shape of the crushed rock particles can be described as ideally spherical.
- The size distributions within each particle diameter interval can be represented by the mean of that interval.

Since there is no established method available for the validation of these assumptions, uncertainty in the resulting sorption has to be acknowledged, although this uncertainty can not be quantified.

For the Laxemar 1.2 site description, preliminary sorption coefficients have been extracted from the on-going investigation programme. Results from the batch sorption experiment using Ävrö granite sampled at KLX03A at 522.61–523.00 m depth. Experiments have been performed with the crushed rock material in contact with fresh groundwater and present groundwater at repository level (Type I and III, respectively). Preliminary results have been extracted from the on-going laboratory experiment programme and have been evaluated according to the concept expressed by Equation 3-3 described above. Consequently, sorption coefficients are available for Cs(I), Sr(II), Ni(II), Ra(II) and Am(III) and these are presented in Table 3-7.

The following observations can be made in the preliminary results:

- The majority of the K_d-values obtained are within the range of the corresponding values in the sorption database provided by /Carbol and Engkvist 1997/. Exceptions are the values given for Am(III), where the values in this report are considerably lower (see comment below) and for Ra(II) in groundwater type III where the value in this report is somewhat lower.
- In the case of Sr(II) in groundwater type III, the sorption was so low that no statistically verifiable concentration decrease could be obtained for the water phase. The K_d value reported (< 2E–2 m^3/kg) corresponds to the lowest measurable R_d.
- For sorption of Cs(I) and Ni(II) in groundwater type III, the extrapolation according to Equation 3-3 gives K_d which, given the uncertainties, can not be statistically verified to be above zero. Therefore, numerical K_a values are presented for these tracers but only the detection limit for K_d (i.e. corresponding to the highest value that statistically can be obtained from the extrapolation according to Equation 3-3).
- In the case of Am(III), it must be considered that in the sorption experiment > 97% of the tracer in the blank sample was lost due to sorption on the test tube walls. According to the procedures described in the method description, the obtained values should therefore be a subject for further investigation and the values presented in this report should therefore be treated with care.

Table 3-7. Experimentally determined sorption coefficients for the Laxemar 1.2 site description according to the process described above. The only available results are from the interaction of Ävrö granite (KLX03A, 522.61–523.00 m) with fresh (Type I) and repository level (Type III) groundwater, cf Table 2-4 for the chemical composition of the different groundwaters. The values are preliminary and are obtained for contact times of one month, exception for Am(II) where a contact time of 3 months is applied. The final values are planned /cf Widestrand et al. 2003/ to be determined for 6 months contact time.

	Fresh groundwater (type I) K_d (m^3/kg)		K_a (m)	Saline groundwater (type III) K_d (m^3/kg)		K_a (m)
Tracer	**Experimental**	**/Carbol and Engkvist 1997/**	**Experimental**	**Experimental**	**/Carbol and Engkvist 1997/**	**Experimental**
Cs(I)	(4.2±3.5)E–2	0.1–1	(2.8±0.3)E–2	< 2E–2	0.01–0.1	(9.5±1.4)E–3
Sr(II)	(5.8±1.4)E–3	0.005–0.05	(8.0±1.3)E–4	< 4E–4	0.0001–0.001	< 2E–5
Ra(II)	(1.4±1.1)E–1	0.05–0.5	(1.9±1.0)E–2	(4.0±3.6)E–3	0.01–0.1	(9.7±3.3)E–4
Ni(II)	(1.3±0.8)E–1	0.05–0.5	(1.8±0.8)E–2	< 2E–2	0.01–0.1	(3.5±0.8)E–3
Am(III)	(1.0±0.5)E–2	1–5	(2.8±0.5)E–3	(1.9±1.5)E–2	1–5	(2.4±1.4)E–3

A considerable drawback of the sorption data is that data are only available for the interaction with Ävrö granite. For the other rock major rock types and for the fracture specific materials, no site-specific experimental sorption data are available. An attempt has therefore been made to use the measured BET-surface values to extrapolate sorption coefficients. These calculations are made using the assumption that the sorption coefficient for a material is directly proportional to the available amount of surfaces. The calculations to obtain a K_d for the rock material (x) have therefore been performed according to:

$$K_{d(x)} = R_{d\,(\text{ÄG 63-125 µm})} \cdot \frac{A_x}{A_{(\text{ÄG 63-125 µm})}} \qquad (3\text{-}4)$$

where $R_{d(\text{ÄG 63–125µm})}$ is the experimentally measured tracer distribution coefficient obtained for the 63–125 µm size fraction of Ävrö granite, $A_{(\text{ÄG 63–125µm})}$ is the measured BET surface area for the same rock type in the size fraction and A_x is the measured BET surface area for the rock material (x). It should be noticed that the BET surface for the different rock types has preferentially been obtained from the extrapolation of inner BET surface according to the procedures described in Section 3.6.1 (results given in the right column in Table 3-6). However, for some rock materials (especially fracture specific materials) only the small size fraction has been measured (63–125µm or < 125µm). For these rock types, the A_x has therefore not been a subject for determination of inner BET surface by extrapolation; instead the measured BET surface area for the small size fraction has been directly inserted as A_x in Equation 3-4.

The results from these BET surface based extrapolations of K_d-values are given in Table 3-8. Very similar values were obtained for the different major rock types. For the fracture and structure element materials building up the deformation zones, significantly high K_d-values are reported, this caused by the high BET areas measured in these samples.

It should be emphasized that this extrapolation is a rather rough method to assign K_d-values to non-measured rock material. For example, in /Allard et al. 1983/ a far from perfect correlation was obtained for the cation exchange capacity to the BET surface area, indicating a more complex and mineral-dependent relationship between sorption capacity and the BET surface area. Nevertheless, in the situation of lacking sorption measurements for the most of the site specific rock types of Laxemar, we consider this concept as the best available method of assigning sorption coefficients to the different materials. In forthcoming versions of the Laxemar site descriptions, more sorption data will be available; this will facilitate further evaluations of the K_d-prediction concept.

Table 3-8. Sorption coefficients obtained from extrapolation of BET surface measurements, see text for details.

Sorption data	Rock type	BET surface (m^2/g)	Groundwater type	Cs(I)	Sr(II)	Ni(II)	Ra(II)	Am(III)
R_d (0.063–0.125 mm)	Ävrö granite	0.25±0.04[A]	III	0.4±0.3	< 0.0003	0.08±0.01	0.023±0.001	0.07±0.01
			I	0.61±0.03	0.022±0.002	0.5±0.2	0.507±0.001	0.069±0.0109
Estimated K_d (m^3/kg)	Ävrö granite	0.04±0.02[B]	III	0.06±0.05	< 5E–5	0.010±0.004	0.003±0.001	0.009±0.004
			I	0.08±0.03	0.003±0.001	0.06±0.04	0.06±0.02	0.009±0.004
	Fine-grained dioritoid	0.06±0.02[B]	III	0.10±0.09	< 9E–5	0.018±0.009	0.005±0.003	0.016±0.010
			I	0.14±0.07	0.005±0.003	0.12±0.07	0.12±0.06	0.017±0.01
	Quartz monzodiorite	0.02±0.02[B]	III	< 0.09	< 4E–5	< 0.015	< 0.005	< 0.0138
			I	< 0.11	< 0.004	< 0.1	< 0.1	< 0.013
	Fine-grained diorite-gabbro	0.06±0.01[B]	III	0.10±0.08	< 9E–05	0.018±0.006	0.005±0.002	0.016±0.006
			I	0.14±0.04	0.005±0.002	0.11±0.06	0.11±0.03	0.016±0.005
	Diorite to gabbro	0.039±0.005[B]	III	0.07±0.06	< 6E–5	0.012±0.003	0.0036±0.0008	0.011±0.003
			I	0.09±0.02	0.0035±0.0008	0.08±0.04	0.08±0.02	0.011±0.003
	Ävrö granite, altered	0.079±0.013	III	0.14±0.11	< 1E–4	0.025±0.007	0.007±0.002	0.022±0.007
			I	0.19±0.04	0.007±0.002	0.16±0.07	0.16±0.04	0.022±0.006
	Fracture B, filling material	2.69±0.07[C]	III	5±4	< 0.004	0.9±0.2	0.25±0.05	0.8±0.2
			I	7±1	0.24±0.05	5±2	5±1	0.7±0.2
	Fracture C	3.3±0.2[B]	III	6±5	< 0.005	1.0±0.3	0.30±0.06	0.9±0.3
			I	8±2	0.30±0.06	7±3	7±1	0.9±0.28
	Fracture D	24.1±0.9[A]	III	40±30	< 0.04	8±2	2.1±0.4	7±2
			I	60±10	2.1±0.4	50±20	50±9	7±15
	Structure element 1/4	24.9±0.6[C]	III	40±30	< 0.04	8±2	2.3±0.4	7±2
			I	60±10	2.2±0.5	50±20	50±9	7±2
	Gouge material, Structure element 1	9.3±0.1[C]	III	16±13	< 0.015	3.0±0.7	0.9±0.2	2.6±0.7
			I	23±4	0.8±0.2	19±8	19±3	2.6±0.6
	Structure element 2	7.89±0.01[B]	III	14±11	< 0.012	2.5±0.6	0.8±0.1	2.2±0.6
			I	19±3	0.7±0.1	16±7	16±3	2.2±0.5

A) Measured using the 0.063–0.125 mm size fraction.
B) Estimate of inner BET surface, extrapolation according to Equation 3-3.
C) Measured using the < 0.125 mm size fraction.

4 Development of retardation model

In accordance with the concept proposed by /Widestrand et al. 2003/, the retardation model should consist of tables in which the geological description and the selected transport parameters for each unit (rock mass or fracture/deformation zone) where retardation of radionuclides can take place are given.

4.1 Methodology

The developed retardation model consists of two parts, one for the major rock types, i.e. for the dominant rock types within the rock domains, and one for the fractures and deformation zones. In the first part, the retention characteristics of the major rock types, i.e. rock matrix interaction parameters, are described. The second part provides a description of the retardation in the water-conducting fractures and deformation zones.

This section lists the parameters presented in the different parts of the model and presents the motivations for the data selections that were made.

4.1.1 Major rock types

According to the retention concept applied in the present work (cf Section 1.2 and Chapter 3), the retardation of radionuclides in the rock matrix is described using the following parameters:

- ***Rock matrix porosity,*** θ_m ***(–):*** The results from the water saturation porosity measurements on site-specific rock materials have been selected in this work (cf Table 3-1). A log-normal distribution has been considered to describe the system somewhat better than a normal distribution (although not perfectly), and has therefore been selected for the representation.
- ***Rock matrix formation factor,*** F_m ***(–):*** This parameter is used to multiply literature values of the radionuclide-specific free diffusivities in water (D_w (m^2/s); tabulated, e.g. by /Ohlsson and Neretnieks 1997/) to obtain the effective diffusivities, D_e (m^2/s), for the different radionuclides. Since the results of the laboratory electrical resistivity measurements are based on a larger number of samples and have been found not to deviate significantly from the through-diffusion results, they have been selected for the retardation model (cf Table 3-6). For consistency with the closely related porosity parameter, a log-normal distribution has been selected also for the formation factor representation.
- ***Rock matrix sorption coefficient,*** K_d ***(m^3/kg):*** This parameter describes the sorption (i.e. radionuclide attachment) on the surfaces on of the pores of the rock material. Experimentally determined data are available for the Ävrö granite rock type, cf Table 3-7. For all the other rock types, estimates are given based on extrapolations from the BET surface area measurements, cf Table 3-8 and referred discussion.

4.1.2 Fractures and deformation zones

The present retention concept proposed by /Widestrand et al. 2003/ shall produce retardation models for the identified fracture and deformation zone types by describing and quantifying the retardation properties of the different layers of geological materials present in and in the immediate vicinity of the fractures/deformation zones. The geological materials in the fractures and deformation zones could consist of, e.g. fault gouge, fracture coating, mylonite and altered wall rock. In the retardation modelling, attempts will be made to give the following parameters for the different layers:

- thickness,
- porosity, θ_m,
- formation factor, F_m (to be used in calculations of the diffusivities of the different radionuclides),
- sorption parameters, i.e. surface distribution coefficients, K_a (m), and/or volumetric distribution coefficients, K_d (m^3/kg),
- mineral contents and, if possible, grain sizes.

In addition, the following data on each particular fracture type will be given:

- abundance (percentage) of the fracture type, i.e. a quantification of how large portion of the entire fracture class the given description is valid for,
- transmissivity interval observed for this particular fracture or deformation zone type,
- preferential direction (if any).

In the L1.2 site description, an identification and quantitative description of different fracture types is presented, whereas minor deformation zone types cannot be identified due to the uncertainties in their classification (Section 2.2.2). The limitations of the presently available dataset lead to that also some parameter values in the tables describing the identified fracture types are missing.

4.2 Retardation model

4.2.1 Major rock types

The geological model is based on rock domains, whereas the sampling for the transport programme is based on rock types and mainly focused on the two major rock types (Ävrö granite and quartz monzodiorite). The samples represent both fresh and altered samples of these rock types. Also minor rock types have been sampled, but no data on these are so far available. The potentially greater importance of the fine-grained granite for transport, indicated by observations of its percentage of open fractures and deviating transport properties /Mazurek et al. 1997, Landström and Tullborg 1993/ and also observed as, e.g. deviations in hydraulic properties, has not been addressed in the present work.

As discussed in previous chapters, large parts of the rock are hydrothermally altered, i.e. secondary red staining (oxidation) and/or saussuritization, which is expected to affect the transport properties. Hydrothermal alteration occurs in both Ävrö granite and quartz monzodiorite as well as in minor rock types.

Table 4-1 presents the selected transport parameters for the fresh and altered major rock types. The percentages quantify the portions of the rock types that are altered; they are estimated from data in the L1.2 geological description /SKB 2006a, Chapter 5/ and Boremap classifications, where only the classes referred to as weak, medium and strong alteration have been considered. The alteration generally seems to be weaker at the Laxemar area compared to the Simpevarp area. However, it has not yet been fully established how to translate degrees of alteration between the two subareas, mainly due to differences in rock types and some uncertainties in the classification.

The parameterisation of the major rock types can then be used to parameterise the different rock domains. Several rock domains constitute the rock volume of the Laxemar subarea. The rock domains consist of mixtures of the different rock types according to Table 4-2, which is based on borehole data from KLX02–KLX06 and represent five of the rock domains.

Table 4-1. Suggested transport parameters for the major rock types at the Laxemar subarea. Parameter values in italics refer to K_d-values that have not been measured for that particular rock type, but instead have been obtained by extrapolation from the results for the BET surface area measurements, cf Table 3-8.

Rock type	Porosity (vol %)	Formation factor (–)	K_d (m^3/kg) (water type I)					K_d (m^3/kg) (water type III)				
			Cs(I)	Sr (II)	Ni(II)	Ra(II)	Am(III)	Cs(I)	Sr (II)	Ni(II)	Ra(II)	Am(III)
Ävrö granite	0.27±0.09	(1.4±1.0)E–4	(4.2±3.5)E–2	(5.8±1.4)E–3	(1.3±0.8)E–1	(1.4±1.1)E–1	(1.0±0.5)E–2	< 2E–2	< 4E–4	(1.1±0.6)E–2	(4.0±3.6)E–3	(1.0±0.5)E–2
Quartz monzodiorite,	0.17±0.08	(3.6±3.5)E–5	*< 0.11*	*< 0.004*	*< 0.1*	*< 0.1*	*< 0.013*	*< 0.09*	*< 4E–5*	*< 0.015*	*< 0.005*	*< 0.014*
Fine-grained dioritoid	0.14±0.14	1E–5[A]	*(1.4±0.7)E–1*	*(5±3)E–3*	*(1.2±0.7)E–1*	*(1.2±0.6)E–1*	*(1.7±1.0)E–2*	*(1.0±0.9)E–1*	*< 1E–4*	*(1.8±0.9)E–2*	*(5±3)E–3*	*(1.7±1.0)E–2*
Fine-grained diotite-gabbro	0.22±0.08	(6.4±4.2)E–5	*(1.4±0.4)E–1*	*(5±2)E–3*	*(1.1±0.6)E–1*	*(1.1±0.3)E–1*	*(1.6±0.5)E–2*	*(1.0±0.8)E–1*	*< 1E–4*	*(1.8±0.6)E–2*	*(5±2)E–3*	*(1.6±0.6)E–2*
Fine-grained granite	0.22±0.0002	No data	No data	No data	No data	No data	No data	No data	No data	No data	No data	No data
Granite	0.38 [A]	8E–5[A]	No data	No data	No data	No data	No data	No data	No data	No data	No data	No data
Diorite to gabbro	No data	No data	*(9±2)E–2*	*(3.5±0.8)E–3*	*(8±4)E–2*	*(8±2)E–2*	*(1.1±0.3)E–2*	*(7±6)E–2*	*< 6E–5*	*(1.2±0.3)E–2*	*(3.6±0.8)E–3*	*(1.1±0.3)E–2*
Altered Ävrö granite (selected to represent all altered wall rock)	No data	No data	*0.19±0.04*	*0.007±0.002*	*0.16±0.07*	*0.16±0.04*	*0.022±0.006*	*0.14±0.11*	*< 1E–4*	*0.025±0.007*	*0.007±0.002*	*0.022±0.007*

A) Data based on a single sample measurement, therefore no uncertainty interval is given.

Table 4-2. Estimated percentages of different rock types in the rock domains of the Laxemar subarea.

Rock domain	Ävrö granite	Quartz monzo-diorite	Fine-grained dioritoid	Fine- to medium-grained granite	Pegmatite	Diorite to gabbro	Fine-grained diorite to gabbro	Granite
RSMA01 [A)]	54–92%	1 –14%	2–21%	1–22%	0–1%	0–12%	0–5%	
RSMD01		95%		4%	0.3%			
RSMBA01	47%		27%		2%		23%	
RSMBA03	57%		32%	1%	1%		8%	1%
RSMM01	38–73%	0–27%		1–16%	0–0.3%	1–36%		0–26%

A) Distribution of rock types in domain RSMA01 is based on boreholes data from both the Laxemar and the Simpevarp area /Wahlgren et al. 2005/.

4.2.2 Fractures

The following simplifications and quantitative estimates are used as a basis for the identification and parameterisation of different fracture types:

Chlorite+calcite is the overall dominating coating in the open fractures. Hematite is present in about 10% of the open fractures, clay minerals in 30% of all open fractures.

According to the presently available data, the presence of different fracture coatings cannot be related to specific rock types. This is important for the application of the identified fracture types in transport models; if present, such relations could provide a basis for assigning different fracture types to the different rock domains.

Concerning the host rock, it is suggested that a significant part of the fractures are situated in altered parts of the rock, although it has been some difficulties to determine the total frequency (cf Chapter 2).

Based on the core mapping only, the following quantification and description of different fracture types is suggested:

A. 40% have chlorite and calcite as fracture coating (max 0.5 mm thick on each side) and fresh wall rock.

B. 20% have chlorite and calcite as fracture coating +/– prehnite, epidote etc (max 1 mm thick on each side) and altered wall rock ≤ 2 cm (on each side of the coating).

C. 10% have chlorite+calcite+hematite as fracture coating (max 1 mm thick on each side); all of these fractures have altered wall rock ≤ 5 cm (on each side of the coating).

D. 30% have chlorite+calcite+clay minerals as fracture coating (max 2 mm thick on each side); all of these fractures have altered wall rock ≤ 5 cm (on each side of the coating).

The quantitative descriptions of the identified fracture types, including the available retardation parameters, are given in Tables 4-3 to 4-6.

The notation “pending” frequently used in the tables indicates that this transport is not available for that geological unit in this version of the site description. These gaps are intended to be filled in the later versions of the site descriptions.

Table 4-3. Retardation model for Fracture type A.

		Fracture coating	Fresh host rock
Distance		Max 0.5 mm	≥ 0.5 mm
Porosity			According to Table 4-1
Formation factor		Pending	According to Table 4-1
Cs, K_d (m^3/kg)	**GW type I**	Pending	According to Table 4-1
	GW type III	Pending	According to Table 4-1
Sr, K_d (m^3/kg)	**GW type I**	Pending	According to Table 4-1
	GW type III	Pending	According to Table 4-1
Ni, K_d (m^3/kg)	**GW type I**	Pending	According to Table 4-1
	GW type III	Pending	According to Table 4-1
Ra, K_d (m^3/kg)	**GW type I**	Pending	According to Table 4-1
	GW type III	Pending	According to Table 4-1
Am, K_d (m^3/kg)	**GW type I**	Pending	According to Table 4-1
	GW type III	Pending	According to Table 4-1
Mineral content		Chlorite, calcite	See geological description
Grain size		Pending	Pending
Proportion of conducting structures		40%	
Transmissivity interval		Pending	
Direction		Pending	

Table 4-4. Retardation model for Fracture type B. Values given in italics represent extrapolations obtained from BET surface measurement.

		Fracture coating	Altered wall rock	Fresh host rock
Distance		0.5–1 mm	2 cm	≥2 cm
Porosity			According to Table 4-1	According to Table 4-1
Formation factor			According to Table 4-1	According to Table 4-1
Cs, K_d (m^3/kg)	**GW type I**	*7±1*	According to Table 4-1	According to Table 4-1
	GW type III	*5±4*	According to Table 4-1	According to Table 4-1
Sr, K_d (m^3/kg)	**GW type I**	*0.24±0.05*	According to Table 4-1	According to Table 4-1
	GW type III	*< 0.004*	According to Table 4-1	According to Table 4-1
Ni, K_d (m^3/kg)	**GW type I**	*5±2*	According to Table 4-1	According to Table 4-1
	GW type III	*0.9±0.2*	According to Table 4-1	According to Table 4-1
Ra, K_d (m^3/kg)	**GW type I**	*5±1*	According to Table 4-1	According to Table 4-1
	GW type III	*0.25±0.05*	According to Table 4-1	According to Table 4-1
Am, K_d (m^3/kg)	**GW type I**	*0.7±0.2*	According to Table 4-1	According to Table 4-1
	GW type III	*0.8±0.2*	According to Table 4-1	According to Table 4-1
Mineral content		Chlorite, calcite ± prehnite, epidote etc	See geological description	See geological description
Grain size		Pending	Pending	Pending
Proportion of conducting structures		20%		
Transmissivity interval		Pending		
Direction		Pending		

Table 4-5. Retardation model for Fracture type C. Values given in italics represent extrapolations obtained from BET surface measurement.

		Fracture coating	Altered wall rock	Fresh host rock
Distance		0.5–1 mm	5 cm	≥5 cm
Porosity		Pending	According to Table 4-1	According to Table 4-1
Formation factor		Pending	According to Table 4-1	According to Table 4-1
Cs, K_d (m^3/kg)	**GW type I**	*8±2*	According to Table 4-1	According to Table 4-1
	GW type III	*6±5*	According to Table 4-1	According to Table 4-1
Sr, K_d (m^3/kg)	**GW type I**	*0.30±0.06*	According to Table 4-1	According to Table 4-1
	GW type III	*< 0.005*	According to Table 4-1	According to Table 4-1
Ni, K_d (m^3/kg)	**GW type I**	*7±3*	According to Table 4-1	According to Table 4-1
	GW type III	*1.0±0.3*	According to Table 4-1	According to Table 4-1
Ra, K_d (m^3/kg)	**GW type I**	*7±1*	According to Table 4-1	According to Table 4-1
	GW type III	*0.30±0.06*	According to Table 4-1	According to Table 4-1
Am, K_d (m^3/kg)	**GW type I**	*0.9±0.3*	According to Table 4-1	According to Table 4-1
	GW type III	*0.9±0.3*	According to Table 4-1	According to Table 4-1
Mineral content		Chlorite, calcite, hematite	See geological description	See geological description
Grain size		Pending	Pending	Pending
Proportion of conducting structures		10%		
Transmissivity interval		Pending		
Direction		Pending		

Table 4-6. Retardation model for Fracture type D. Values given in italics represent extrapolations obtained from BET surface measurement.

		Fracture coating	Altered wall rock	Fresh host rock
Distance		1–2 mm	5 cm	≥5 cm
Porosity		Pending	According to Table 4-1	According to Table 4-1
Formation factor		Pending	According to Table 4-1	According to Table 4-1
Cs, K_d (m^3/kg)	**GW type I**	*60±10*	According to Table 4-1	According to Table 4-1
	GW type III	*40±30*	According to Table 4-1	According to Table 4-1
Sr, K_d (m^3/kg)	**GW type I**	*2.1±0.4*	According to Table 4-1	According to Table 4-1
	GW type III	*< 0.04*	According to Table 4-1	According to Table 4-1
Ni, K_d (m^3/kg)	**GW type I**	*50±20*	According to Table 4-1	According to Table 4-1
	GW type III	*8±2*	According to Table 4-1	According to Table 4-1
Ra, K_d (m^3/kg)	**GW type I**	*50±9*	According to Table 4-1	According to Table 4-1
	GW type III	*2.1±0.4*	According to Table 4-1	According to Table 4-1
Am, K_d (m^3/kg)	**GW type I**	*7±2*	According to Table 4-1	According to Table 4-1
	GW type III	*7±2*	According to Table 4-1	According to Table 4-1
Mineral content		Chlorite, calcite, clay minerals	See geological description	See geological description
Grain size		Pending	Pending	Pending
Proportion of conducting structures		30%		
Transmissivity interval		Pending		
Direction		Pending		

4.2.3 Deformation zones

Based on the information available at this stage in the site investigation, it is not possible to provide a retardation model for the local minor and major deformation zones. This is primarily due to the lack of transport data hitherto, but also to uncertainties in the classification of minor deformation zones (Section 2.2.2). The only data available so far are BET-measurements; porosity (including PMMA), diffusion and sorption measurements are still in progress.

A few things can, however, be pointed out:

- The local minor deformation zones are hosted in altered rocks, with various amounts of fault gouge and cataclasite.
- Chlorite- and clay-rich zones (on the order of < 1 cm), hosted in altered wall rock (dm-wide), are also found.
- The available data are too limited to allow conclusions on the abundances of different types of deformation zones.

4.3 Application of the retardation model

Tables 4-1 and 4-2 provide a basis for parameterisation of the rock domains RSMA01, RSMBA01, RSMBA03, RSMD01 and RSMM01. The parameterisation of each rock domain could range from a simple selection of a single parameter value for the dominant rock type in that domain to, for instance, volume averaging using data for fresh or altered rock, or both. For the diffusion parameters of the major rock types, statistical distributions are given that can be used as a basis for stochastic parameterisation of transport models.

At this stage of model development, the retardation model should be viewed as a presentation of the interpreted site-specific information on retardation parameters, intended to provide a basis for the formulation of alternative parameterisations within the Safety Assessment modelling.

The quantitative descriptions of the identified fracture types, including the available retardation parameters, are given in Tables 4-3 to 4-6. The fracture types in the present retardation model could be used as a basis for modelling radionuclide transport along flow paths in the fractured medium. However, the model could also be viewed as primarily proposing a basic structure, for discussion and further development, which from the viewpoint of numerical transport modelling will become more useful when more data are at hand.

Concerning the parameterisation of flow paths in transport models, it should also be noted that at present there are no data supporting, for instance, quantitative correlations between fracture types and hydraulic properties. Furthermore, it could be observed that the present data indicate that the presence of different fracture coatings cannot be related to specific rock types. No identification or description of the deformation zone types is given in the present model.

4.4 Evidence from process-based modelling

As discussed in Section 1.2.2, alternative retention processes and process models are considered within the site descriptive transport modelling, so far mainly in the form of process-based sorption models. It is expected that the results of this modelling will be useful for supporting, or providing alternatives to, the K_d-based sorption model regarding actual parameter values as well as for the understanding of the site-specific sorption processes in general. However, no results that can be used for these purposes are presently available.

4.5 Evaluation of uncertainties

General discussions on the uncertainties related to the site-descriptive transport model are given in the transport modelling guidelines /Berglund and Selroos 2004/. Similar to the other geoscientific disciplines, spatial variability is considered an important potential source of uncertainty in the modelling of transport properties. Quantitative results from previous studies on Äspö HRL /Byegård et al. 1998, 2001, Löfgren and Neretnieks 2003, Xu and Wörman 1998/, demonstrating spatial variability along flow paths and within the matrix, are briefly summarised in /SKB 2004/.

A major uncertainty identified in the previous site descriptions, see /Byegård et al. 2005ab/, is related to varying degrees of absence of site-specific transport data. As described in the present report, this uncertainty has been largely resolved in the L1.2 model, especially due to the addressing of site specific sorption coefficient data. However, some significant data gaps still remain, especially concerning the transport parameters (porosity, diffusivity and sorption coefficients) for materials in fractures and deformation zones. Furthermore, the available data are still insufficient for establishing quantitative relations between transport parameters and other properties of fractures and deformation zones, e.g. lengths, orientations and hydraulic properties.

The uncertainties considered most relevant for the present description of transport properties can be categorised as follows:

- Uncertainties in the data and models obtained from other disciplines, primarily Geology and Hydrogeochemistry.
- Uncertainties in the interpretations and use of data and models from other disciplines, i.e. in interpretations of the relations between transport properties and various underlying properties, and the simplifications made in the identification and parameterisation of "typical" matrix materials and fractures.
- Data uncertainties related to measurements and spatial variability of transport parameters, including the "extrapolation" of small-scale measurements to relevant model scales.
- Conceptual uncertainties related to transport-specific processes and process models.

This model provides quantitative information on transport data uncertainties only. Uncertainty ranges, in most cases taken directly from the experimental data, are given in the data tables above. Essentially, these ranges incorporate both random measurement errors and the spatial variability associated with the particular dataset.

The uncertainties introduced by the inputs from other disciplines and by the "expert judgement" utilised to interpret and use these data have not been addressed in the transport description. Whereas the uncertainties in the descriptions devised by Geology and Hydrogeochemistry are discussed in the L1.2 SDM report /SKB 2006a/, Chapters 5 and 9, respectively, no attempt has been made to formulate alternative interpretations or otherwise address the "expert judgment" aspects of this work. It can be noted, however, that the differences in parameter values between, e.g. different rock types give some indications on the possible ranges of these uncertainties.

Regarding the uncertainties related to spatial variability and scale, it may be noted that some measurements providing data to the retardation model (e.g. porosity, BET surface area and sorption) have been obtained in the laboratory, on a millimetre- to centimetre-scale. The proper means of "upscaling" these parameters is by integrating them along flow paths in groundwater flow models, implying that the scale of the flow model is the relevant model scale. The approach is here to present the data on the measurement scale, thereby providing a basis for further analysis in connection with the numerical flow and transport modelling.

5 Summary and implications for further studies

5.1 Summary of observations

Site investigation data from porosity measurements, diffusion experiments, formation factor evaluation (in situ and in the laboratory) and sorption coefficients have been available for the L1.2 modelling. The modelling work included evaluations of data on rock mass geology and fractures, and hydrogeochemistry, in addition to the evaluation of transport data.
The main observations from the evaluations of transport data and information from other disciplines can be summarised as follows:

- The major rock types of the Laxemar subarea are Quartz monzodiorite and Ävrö granite. Compared with the Simpevarp subarea the proportions of altered rock are lower /Byegård et al. 2005a/. Since the majority of the rock samples for resistivity and diffusivity measurements were taken from boreholes KLX02 and KLX04 (the northern part of the Laxemar subarea) there is a predominance of data for the Ävrö granite for the rock used so far in the investigations.
- However altered rock is common along water conducting fractures and deformations zones. This means that transport in the open fractures to large extent takes place in the altered parts of the rock.
- Fracture fillings in the hydraulically conductive fractures are, in addition to chlorite and calcite, often clay minerals which are present as outermost coatings. Larger structures usually carry various amounts of gouge material. Hematite is present in 4–9% of the conductive fractures. Hydrothermal Al-silicates like prehnite, epidote and adularia are common but subordinate and not expected to give significant contributions to the sorption capacity.
- The presence of different fracture coatings is not related to the rock type in the investigated boreholes in the Laxemar area.
- Bore map data from KLX03 and KLX04 shows total number of fractures amounting to 4,388 (KLX03) and 5,498 (KLX04). Of these 15% and 36%, respectively, are mapped as open fractures. Evaluation of flow log measurements correlated with Bore map data /Rhen et al. 2005/ shows that approximately 2% (KLX03) and 5% (KLX04) of the total number of fractures are hydraulically conductive and show transmissivities above10^{-9} m/s. The definition of the open conductive fractures versus rock mass is crucial for the transport modelling. The parameterisation of the rock mass in between the fractures is dependent on assumptions made of the number of the open fractures that are included in the transport modelling as flowing structures, in that the rest of the fractures (the sealed and the open without flow) will contribute to the properties of the rock mass with a higher porosity and preferred diffusion pathways. This will be further elaborated in forth coming model versions of the transport properties parameterisation. The fracture frequency at the Laxemar site is all together lower compared to the Simpevarp site; although a large variation of fracture frequencies is observed for the Laxemar site.
- The hydrochemistry in the Laxemar subarea is characterised by fresh water (of present meteoric and glacial water origins) at depth interacting with deep saline groundwater. Based on observations from boreholes KLX03 and KLX04 the salinity at repository depth is approximately 1,300–2,000 ppm Cl. The water compositions used in most of the batch sorption experiments are fresh diluted Ca-HCO_3 (I) and groundwater of Na-Ca-Cl type (8,800 mg/L Cl) (III). The water types were chosen before hydrochemical information from KLX03 and KLX04 was available.

- Porosity data, measured as water saturation, from the major rock types show mean values between 0.26–0.32% and for rock samples without alterations or visible cracks 0.17–0.27%. However, for several of the rock types, the standard deviation within the population of samples used is overlaps the given intervals above. The Ävrö granite shows the highest mean values for both fresh and altered samples. For the Simpevarp data set, mean values were in the range of 0.21–0.42% and 0.17–0.40% when excluding samples with alteration and/or visible cracks.
- Most of the through diffusion measurements are ongoing and have not reached steady state yet. However, the preliminary results indicate a general consistency with the laboratory resistivity measurements, possibly with the through diffusion results giving somewhat lower formation factors than laboratory resistivity measurements. The preliminary formation factors for the Ävrö granite (with the exception of the very coarse grained variety) are in the range of 7.5E–6 to 1.4E–5 based on through diffusion whereas laboratory resistivity measurements yielded mean values of (1.4±1.0)E–4. This can be compared to the corresponding values evaluated from the Simpevarp data set /SKB 2005/; (5.3±0.6)E–4 for through diffusion and (2.9±2.9)E–4 for laboratory resistivity measurements. For the Quartz monzodiorite the preliminary through diffusion results showed values between 5.6 E–6 to 3.1E–5 and based on laboratory resistivity measurements (3±3)E–5. In the Simpevarp data set, no values were given for through diffusion experiments using Quartz monzodiorite while the laboratory resistivity measurements gave formation factors in the range of (1.1±1.6)E–4.
- BET surface measurements on crushed rock and fracture filling material have been carried out and show an order of 10 to 100 times higher BET surfaces for the fracture material.
- Preliminary sorption coefficients for Ävrö granite sampled at KLX03A at 522.61–523.00 m depth have been extracted from the investigation programme. Experiments have been performed with crushed rock material in contact with fresh and saline groundwaters (Type I and III, respectively). The sorption coefficients available for Cs(I), Sr(II), Ni(II), Ra(II) and Am(III) are in accordance with the previously compiled sorption data for use in the Sr-97 safety assessment /Carbol and Engkvist 1997/ except for Am (III) which showed lower K_d compared with the database values.

5.2 Retardation model

A retardation model (cf Tables 4-1 to 4-6) was developed in accordance with the proposed modelling strategy /Widestrand et al. 2003, Berglund and Selroos 2004/. The retardation model contains data for the fresh and altered forms of the major rock types in the Laxemar subarea (Ävrö granite, quartz monzodiorite and fine-grained dioritoid). Specifically, the retardation model is based on porosity data from water saturation measurements on site-specific rock samples, diffusivities from formation factors measured in laboratory electrical resistivity measurements on site-specific samples, and sorption coefficients for which the majority have been based on extrapolations of the results of the BET surface measurements. The sorption dataset is limited to Cs(I), Sr(II), Ra(II), Ni(II) and Am(II) under hydrochemical conditions corresponding to “Groundwater type I” (fresh groundwater) and “Groundwater type III” (saline groundwater).

As a basis for detailed parameterisations of the rock domains, estimated percentages of the major rock types within the rock domains RSMA01, RSMD01, RSMBA01, RSMBA03 and RSMM01 are presented (Table 4-2; data from Geology). Estimated proportions of fresh and altered rock for the largest rock domains within the target area (i.e. RSMA01and RSMD01) are also given. In principle, the parameterisation of each rock domain could range from a simple selection of a single parameter value representing the dominant rock type in that domain to, for instance, volume averaging using data for fresh or altered rock, or both. For the diffusion parameters of the major rock types, statistical distributions are also given.

Four different fracture types have been identified and described in the retardation model, see Tables 4-3 to 4-6. These fracture types include fractures with fracture coating on fresh rock (Fracture type A) and fractures with altered wall rock between the coating and the fresh rock (Fracture types B, C and D). The estimated percentages of the different fracture types (proportions of all open fractures) are also given. However, it should be noted that retardation parameters are not available for all materials in the model, and that quantitative relations between fracture types and other properties of the fractures (e.g. lengths, orientations and hydraulic parameters) have not been established.

Although somewhat limited in terms of data and correlations to other parameters and properties of the system, the presented model can be used as a basis for parameterisation of numerical transport models and, perhaps more important, as a basic structure that can be subject to further discussions and development. Concerning the parameterisation of transport models, it could be observed that the present data show that the presence of different fracture coatings cannot be related to specific rock types. No identification or description of fracture zone types is given in the present model. However, the available information and indications related to fracture zones are described in Section 4.2.3.

5.3 Implications for further studies

The present summary and evaluation of site-specific retardation data from Laxemar shows that some types of site data still are missing in the site database. In particular, sorption parameters are only available for the Ävrö granite. However, additional samples from the Laxemar rock cores are a presently measured for sorption and diffusion. This means that the site-specific database will be improved during 2006, filling data gaps identified in the L1.2 model.

Altered and intact varieties of the same rock type may have significantly different transport properties. More data and modelling are needed in order to verify or exclude such differences. The on-going site investigation programme will provide more data on altered and fracture-filling materials, which improves the basis for parameterisation of fractures and deformation zones. It should, however, be acknowledged that the Safety Assessment modelling in the present stage only deals with data for intact rock; therefore, the lack of data for the fracture materials is presently not considered a critical issue.

An important consideration is the potential role of the minor rock types, including fine- to medium-grained granite, fine-grained diorite/gabbro and diorite/gabbro.

The nomenclature concerning fractures and deformation zones needs to be discussed in connection with forthcoming modelling activities, especially for the identification and parameterisation fracture and minor deformation zone types. It has been shown that mapped crush zones overlap with the single factures in terms of transmissivity; there is a grey area between what is defined as single fractures and minor zones for transport modelling purpose.

Thus, the criteria guiding the separation of fractures and minor deformation zones need to be discussed. In a similar way the separation of fractures versus rock mass needs consideration. The incorporation of sealed fractures and a portion of the open but not transmissive fractures into the rock mass may speak in favour of adjustments of the rock mass properties cf for example /Löfgren and Neretnieks 2005/ found a 2–4 times larger formation factor in the fractured rock compared with sections without no identified fractures.

6 References

Allard B, Karlsson M, Tullborg E-L, Larsson S-Å, 1983. Ion exchange capacity and surface areas of some major components and common fracture filling materials of igneous rock. SKB TR 83-64, Svensk Kärnbränslehantering AB.

Berglund S, Selroos J-O, 2004. Transport properties site descriptive model – Guidelines for evaluation and modelling. SKB R-03-09, Svensk Kärnbränslehantering AB.

Brunauer S, Emmet P H, Teller E, 1938. Adsorption of gases in multimolecular layers. J. Am. Chem. Soc., 60: 309-319.

Byegård J, Johansson H, Skålberg M, Tullborg E-L, 1998. The interaction of sorbing and non-sorbing tracers with different Äspö rock types – Sorption and diffusion experiments in the laboratory scale. SKB TR 98-18, Svensk Kärnbränslehantering AB.

Byegård J, Widestrand H, Skålberg M, Tullborg E-L, Siitari-Kauppi M, 2001. Complementary investigation of diffusivity, porosity and sorptivity of Feature A-site specific geological material. SKB ICR-01-04, Svensk Kärnbränslehantering AB.

Byegård J, Gustavsson E, Tullborg E-L, Berglund S, 2005a. Bedrock transport properties. Preliminary site description Simpevarp subarea – version 1.2. SKB R-05-05, Svensk Kärnbränslehantering AB.

Byegård J, Gustavsson E, Tullborg E-L, Selroos J-O, 2005b. Bedrock transport properties. Preliminary site description Forsmark area – version 1.2. SKB R-05-86, Svensk Kärnbränslehantering AB.

Carbol P, Engkvist I, 1997. Compilation of radionuclide sorption coefficients for performance assessment. SKB R-97-13, Svensk Kärnbränslehantering AB.

Crank, J, 1975. The mathematics of diffusion, 2nd ed. Oxford University Press, New York.

Crawford J, 2006. Modelling in support of bedrock transport property assessment. SKB R-06-28, Svensk Kärnbränslehantering AB.

Dershowitz W, Winberg A, Hermanson J, Byegård J, Tullborg E-L, Andersson P, Mazurek M, 2003. Äspö Hard Rock Laboratory. Äspö Task Force on modelling of groundwater flow and transport of solutes – Task 6C – A semi-synthetic model of block scale conductive structures at the Äspö HRL. SKB IPR-03-13, Svensk Kärnbränslehantering AB.

Drake H, Tullborg E-L, 2004. Oskarshamn site investigation. Fracture mineralogy and wall rock alteration. Results from drill core KSH01A+B. SKB P-04-250, Svensk Kärnbränslehantering AB.

Drake H, Tullborg E-L, 2005. Oskarshamn site investigation. Fracture mineralogy and wall rock alteration. Results from drill cores KAS04, KA1755A and KLX02. SKB P-05-174, Svensk Kärnbränslehantering AB.

Drake H, Tullborg E-L, 2006a. Mineralogical, chemical and redox features of red-staining adjacent to fractures – Results from drill cores KSH01A+B and KSH03A+B. SKB P-06-01, Svensk Kärnbränslehantering AB.

Drake H, Tullborg E-L, 2006b. Mineralogical, chemical and redox features of red-staining adjacent to fractures – Results from drill core KLX04. SKB P-06-02, Svensk Kärnbränslehantering AB.

Ehrenborg J, Dahlin P, 2005. Oskarshamn site investigation. Boremap mapping of core drilled borehole KLX03. SKB P-05-24. Svensk Kärnbränslehantering AB.

Ehrenborg J, Dahlin P, 2005. Oskarshamn site investigation . Boremap mapping of core drilled borehole KLX63. SKB P-05-185, Svensk Kärnbränslehantering AB.

Eliasson T, 1993. Mineralogy, geochemistry and petrophysics of red coloured granite adjacent to fractures. SKB TR-93-06, Svensk Kärnbränslehantering AB.

Forssman I, Zetterlund M, Forsmark T, Rhén I, 2005. Correlation of Posiva Flow Log anomalies to core mapped features in KLX02, KLX03, KLX04, KAV04A and KAV04B. SKB P-05-241, Svensk Kärnbränslehantering AB.

Gustavsson E, Börjesson, 2005. Oskarshamn site investigation. Laboratory data from the site investigation programme for the transport properties of the rock. Data delivery for data freeze Laxemar 2.1. SKB P-05-106, Svensk Kärnbränslehantering AB.

Hellmuth K H, Siitari-Kauppi M, Lindberg A, 1993. Study of porosity and migration pathways in crystalline rock by impregnation with 14C-polymethylmethacrylate. J. Cont. Hydrol., 13: 403-418.

Hellmuth K H, Lukkarinen S, Siitari-Kauppi M, 1994. Rock matrix studies with carbon-14-polymethylmethacrylate (PMMA). Method, development and applications. Isotopenpraxis Environ. Health Stud., 30: 47-60.

Jakobsson, 1999. Measurement and modelling using surface complexation of cation (II to IV) sorption onto mineral oxides. Ph.D. Thesis. Department of Nuclear Chemistry, Chalmers University of Technology, Göteborg, Sweden.

Johansson H, 2000. Retardation of tracers in crystalline rock. Ph.D. Thesis. Department of Nuclear Chemistry, Chalmers University of Technology, Göteborg, Sweden.

Johansson H, Byegård J, Skarnemark G, Skålberg M, 1997. Matrix diffusion of some alkali and alkaline earth metals in granitic rock. Mat. Res. Soc. Symp. Proc. 465: 871-878.

Landström O, Tullborg E-L, 1993. Results from a geochemical study of zone NE-1, based on samples from the Äspö tunnel and drillcore KAS 16 (395 to 451 m). SKB Progress Report 25-93-01, Svensk Kärnbränslehantering AB.

Li Y-H, Gregory S, 1974. Diffusion of ions in sea water and in deep sea sediments, Geochim. et Cosmochim. Acta 47: 703-714.

Löfgren M, 2001. Formation factor logging in igneous rock by electrical methods. Licentiate thesis, Department of Chemical Engineering and Technology, Division of Chemical Engineering, Royal Institute of Technology, Stockholm, Sweden.

Löfgren M, Neretnieks I, 2003. Formation factor logging by electrical methods. Comparison of formation factor logs obtained in situ and in the laboratory. J. Contam. Hydrol. 61: 107-115.

Löfgren M, Neretnieks I, 2005. Oskarshamns site investigation. Formation factor logging in-situ by electrical methods in KLX03 and KLX04. SKB P-05-105, Svensk Kärnbränslehantering AB.

Mazurek M, Bossart P, Eliasson T, 1997. Classification and characterisation of water conduction features at Äspö : Results of investigations on the outcrop scale. SKB Äspö Hard Rock Laboratory, ICR-97-01, Svensk Kärnbränslehantering AB.

Munier R, 1993. Segmentation, fragmentation and jostling of the Baltic shield with time. Thesis, Acta Universitatus Upsaliensis 37, Uppsala, Sweden.

Ohlsson Y, Neretnieks I, 1997. Diffusion data in granite – Recommended values. SKB TR-97-20, Svensk Kärnbränslehantering AB.

Parkhomenko E I, 1967. Electrical properties of rocks. Moscow, Institute of Physics of the Earth, Academy of the Sciences of the USSR, 277 p.

Poteri A, Billaux D, Dershowitz W, Gomez-Hernandez JJ, Cvetkovic V, Hautojärvi A, Holton D, Medina A, Winberg A (ed.), 2002. Final report of the TRUE Block Scale project. 3. Modelling of flow and transport. SKB TR-02-15, Svensk Kärnbränslehantering AB.

Rhén I, Forsmark T, Forsman I, Zetterlund M, 2006. Evaluation of hydrogeological properties for Hydraulic Conductor Domains (HCD) and Hydraulic Rock Domains (HRD). Preliminary site description Laxemar subarea – version 1.2. SKB R-06-22, Svensk Kärnbränslehantering AB.

SKB, 2004. Preliminary site description. Simpevarp area – version 1.1. SKB R-04-25, Svensk Kärnbränslehantering AB.

SKB, 2005. Preliminary site description. Simpevarp subarea – version 1.2. SKB R-05-08, Svensk Kärnbränslehantering AB.

SKB, 2006a. Preliminary site description. Laxemar subarea – version 1.2. SKB R-06-10, Svensk Kärnbränslehantering AB.

SKB, 2006b. Hydrogeochemical evaluation. Preliminary site description Laxemar subarea – version 1.2. SKB R-06-12, Svensk Kärnbränslehantering AB.

Stråhle A, 2001. Definition och beskrivning av parametrar för geologisk, geofysisk och bergmekanisk kartering av berget. SKB R-01-19, Svensk Kärnbränslehantering AB.

Thunehed H, 2005a. Oskarshamn site investigation. Resistivity measurements on samples from KLX02. SKB P-05-19, Svensk Kärnbränslehantering AB

Thunehed H, 2005b. Oskarshamn site investigation. Resistivity measurements and determination of formation factors on samples from KLX04 and KSH02. SKB P-05-75, Svensk Kärnbränslehantering AB.

Wahlgren C-H, Hermanson J, Curtis P, Forssberg O, Triumf C-A, Tullborg E-L, Drake H, 2005. Geological description of rock domains and deformation zones in the Simpevarp and Laxemar subareas. Preliminary site description Laxemar subarea – version 1.2. SKB R-05-69, Svensk Kärnbränslehantering AB.

Widestrand H, Byegård J, Ohlsson Y, Tullborg E-L, 2003. Strategy for the use of laboratory methods in the site investigations programme for the transport properties of the rock. SKB R-03-20, Svensk Kärnbränslehantering AB.

Winberg A, Hermansson J, Tullborg, E-L, Staub I, 2003. Äspö Hard Rock Laboratory. Long term diffusion experiment, Structural model of the LTDE site and detailed description of the characteristics of the experimental volume including target structure and intact rock section, SKB IPR-03-51, Svensk Kärnbränslehantering AB.

Winberg A, Andersson P, Hermansson J, Byegård J, Cvetkovic V, Birgersson L, 2000. Äspö Hard Rock Laboratory. Final report on the first stage of the tracer retention understanding experiments. SKB TR-00-07, Svensk Kärnbränslehantering AB.

Xu S, Wörman A, 1998. Statistical patterns of geochemistry in crystalline rock and effect of sorption kinetics on radionuclide migration. SKI Technical Report 98:41, Statens kärnkraftinspektion.

Appendix 1

Porosity data

Results of porosity measurements on samples taken for laboratory through-diffusion and batch-sorption experiments. Measurements are performed according to SS-EN 1936 except for the values presented for KLX02 and given in italics, which originate from /Löfgren 2001/ where a description of the method used is given.

Table A1-1. Porosity data from KLX02.

Borehole	Secup	Seclow	Rock_type	Porosity (%)
KLX02	201.89	201.92	Ävrö granite	0.30
KLX02	216.69	216.7	Ävrö granite	0.35
KLX02	216.7	216.71	Ävrö granite	0.23
KLX02	216.71	216.74	Ävrö granite	0.13
KLX02	216.74	216.79	Ävrö granite	0.15
KLX02	216.79	216.8	Ävrö granite	0.44
KLX02	216.8	216.81	Ävrö granite	0.28
KLX02	216.81	216.84	Ävrö granite	0.19
KLX02	216.84	216.89	Ävrö granite	0.16
KLX02	216.89	216.9	Ävrö granite	0.43
KLX02	216.91	216.92	Ävrö granite	0.33
KLX02	216.92	216.95	Ävrö granite	0.21
KLX02	216.95	217.00	Ävrö granite	0.19
KLX02	220.11	220.14	Ävrö granite	0.36
KLX02	235.02	235.05	Ävrö granite	0.36
KLX02	235.05	235.08	Ävrö granite	0.39
KLX02	235.08	235.11	Ävrö granite	0.39
KLX02	239.88	239.91	Ävrö granite	0.28
KLX02	258.96	258.99	Ävrö granite	0.23
KLX02	280.01	280.04	Ävrö granite	0.19
KLX02	299.79	299.82	Ävrö granite	0.21
KLX02	320.04	320.07	Ävrö granite	0.13
KLX02	339.95	339.98	Ävrö granite	0.17
KLX02	349.16	349.18	Ävrö granite	0.29
KLX02	349.21	349.23	Ävrö granite	0.29
KLX02	350.62	350.64	Ävrö granite	0.38
KLX02	350.66	350.68	Ävrö granite	0.31
KLX02	351.35	351.37	Ävrö granite	0.27
KLX02	351.4	351.42	Ävrö granite	0.32
KLX02	352.53	352.55	Ävrö granite	0.27
KLX02	352.57	352.59	Ävrö granite	0.27
KLX02	353.56	353.58	Ävrö granite	0.28
KLX02	353.57	353.59	Ävrö granite	0.26
KLX02	354.8	354.82	Ävrö granite	0.21
KLX02	354.82	354.84	Ävrö granite	0.19
KLX02	354.84	354.86	Ävrö granite	0.20

Borehole	Secup	Seclow	Rock_type	Porosity (%)
KLX02	354.86	354.88	Ävrö granite	0.20
KLX02	354.88	354.90	Ävrö granite	0.21
KLX02	354.89	354.91	Ävrö granite	0.19
KLX02	354.92	354.94	Ävrö granite	0.18
KLX02	354.93	354.95	Ävrö granite	0.15
KLX02	354.95	354.97	Ävrö granite	0.14
KLX02	354.97	354.99	Ävrö granite	0.16
KLX02	354.99	355.01	Ävrö granite	0.15
KLX02	355.01	355.03	Ävrö granite	0.16
KLX02	355.03	355.05	Ävrö granite	0.16
KLX02	355.05	355.07	Ävrö granite	0.14
KLX02	355.07	355.09	Ävrö granite	0.15
KLX02	355.08	355.10	Ävrö granite	0.14
KLX02	355.1	355.12	Ävrö granite	0.17
KLX02	355.12	355.14	Ävrö granite	0.16
KLX02	355.14	355.16	Ävrö granite	0.14
KLX02	355.16	355.18	Ävrö granite	0.14
KLX02	355.18	355.20	Ävrö granite	0.15
KLX02	358	358.02	Fine-grained diorite-gabbro	0.25
KLX02	359.05	359.07	Ävrö granite	0.33
KLX02	360.46	360.47	Ävrö granite	0.25
KLX02	362	362.02	Ävrö granite	0.32
KLX02	362.06	362.07	Ävrö granite	0.35
KLX02	363.22	363.24	Ävrö granite	0.26
KLX02	363.29	363.31	Ävrö granite	0.27
KLX02	364.3	364.32	Ävrö granite	1.05
KLX02	365.79	365.80	Ävrö granite	0.3
KLX02	365.85	365.87	Ävrö granite	0.29
KLX02	367.12	367.14	Ävrö granite	0.32
KLX02	369.08	369.10	Ävrö granite	0.34
KLX02	369.09	369.11	Ävrö granite	0.3
KLX02	371.66	371.68	Ävrö granite	0.43
KLX02	372.77	372.79	Ävrö granite	0.3
KLX02	372.84	372.86	Ävrö granite	0.34
KLX02	373.93	373.94	Ävrö granite	0.32
KLX02	373.94	373.95	Ävrö granite	0.32
KLX02	375.05	375.07	Ävrö granite	0.31
KLX02	375.07	375.08	Ävrö granite	0.3
KLX02	376.06	376.08	Ävrö granite	0.32
KLX02	376.11	376.13	Ävrö granite	0.33
KLX02	378.13	378.15	Ävrö granite	0.37
KLX02	378.17	378.19	Ävrö granite	0.35
KLX02	381.64	381.66	Ävrö granite	0.3
KLX02	381.71	381.73	Ävrö granite	0.31
KLX02	383.9	383.91	Ävrö granite	0.28
KLX02	383.94	383.96	Ävrö granite	0.25
KLX02	384.41	384.43	Ävrö granite	0.13
KLX02	384.44	384.46	Ävrö granite	0.08

Borehole	Secup	Seclow	Rock_type	Porosity (%)
KLX02	386.07	386.09	Fine-grained diorite-gabbro	0.38
KLX02	386.11	386.13	Fine-grained diorite-gabbro	0.22
KLX02	387.78	387.81	Ävrö granite	0.36
KLX02	388.75	388.76	Fine-grained diorite-gabbro	0.16
KLX02	390.37	390.39	Ävrö granite	0.29
KLX02	390.43	390.45	Ävrö granite	0.3
KLX02	392.4	392.42	Ävrö granite	0.31
KLX02	392.46	392.48	Ävrö granite	0.32
KLX02	395.51	395.53	Ävrö granite	0.34
KLX02	395.59	395.61	Ävrö granite	0.33
KLX02	398.33	398.35	Ävrö granite	0.3
KLX02	398.38	398.40	Ävrö granite	0.3
KLX02	420.02	420.05	Ävrö granite	0.25
KLX02	440.21	440.24	Ävrö granite	0.15
KLX02	459.69	459.72	Ävrö granite	0.38
KLX02	480.02	480.05	Ävrö granite	0.40
KLX02	499.95	499.98	Ävrö granite	0.25
KLX02	519.63	519.66	Ävrö granite	0.21
KLX02	540.03	540.06	Ävrö granite	0.29
KLX02	560.72	560.75	Ävrö granite	0.43
KLX02	579.77	579.8	Ävrö granite	0.30
KLX02	600.19	600.22	Ävrö granite	0.27
KLX02	620.79	620.82	Ävrö granite	0.34
KLX02	639.93	639.96	Ävrö granite	0.42
KLX02	680.83	680.86	Ävrö granite	0.27
KLX02	682.34	682.37	Fine-grained dioritoid	0.06
KLX02	682.37	682.4	Fine-grained dioritoid	0.06
KLX02	682.4	682.43	Fine-grained dioritoid	0.12
KLX02	700.15	700.18	Fine-grained dioritoid	1.49
KLX02	732.47	732.49	Ävrö granite	0.48
KLX02	752.97	752.99	Ävrö granite	0.36
KLX02	776.62	776.64	Ävrö granite	0.30
KLX02	796.14	796.16	Ävrö granite	0.46
KLX02	839.39	839.42	Fine-grained diorite-gabbro	0.15
KLX02	859.7	859.73	Ävrö granite	0.42
KLX02	880.95	880.98	Ävrö granite	1.12
KLX02	898.04	898.07	Fine-grained dioritoid	0.04
KLX02	921.15	921.18	Fine-grained dioritoid	0.07
KLX02	938.42	938.45	Ävrö granite	0.39
KLX02	959.56	959.59	Ävrö granite	0.32
KLX02	979.92	979.95	Ävrö granite	0.41
KLX02	998.2	998.23	Ävrö granite	0.25

Table A1-2. Porosity data from KLX03.

Borehole	Secup	Seclow	Rock_type	Porosity (%)
KLX03	662.10	662.13	Quartz monzodiorite	0.78
KLX03	662.13	662.16	Quartz monzodiorite	0.76
KLX03	662.16	662.19	Quartz monzodiorite	1.03

Table A1-3. Porosity data from KLX04.

Borehole	Secup	Seclow	Rock_type	Porosity (%)
KLX04	110.40	110.43	Ävrö granite	0.24
KLX04	130.55	130.58	Ävrö granite	0.46
KLX04	149.56	149.59	Ävrö granite	0.27
KLX04	169.66	169.69	Granite	0.38
KLX04	190.62	190.65	Ävrö granite	0.39
KLX04	209.72	209.75	Ävrö granite	0.36
KLX04	236.78	236.81	Ävrö granite	0.99
KLX04	256.72	256.75	Ävrö granite	0.43
KLX04	277.66	277.69	Fine-grained dioritoid	0.39
KLX04	297.06	297.09	Ävrö granite	0.89
KLX04	317.19	317.22	Ävrö granite	0.36
KLX04	337.55	337.58	Ävrö granite	0.22
KLX04	357.06	357.09	Ävrö granite	0.36
KLX04	380.78	380.81	Ävrö granite	0.63
KLX04	400.72	400.75	Quartz monzodiorite	0.19
KLX04	419.95	419.98	Granite	0.84
KLX04	460.09	460.12	Quartz monzodiorite	0.12
KLX04	479.82	479.85	Quartz monzodiorite	0.21
KLX04	489.48	489.49	Quartz monzodiorite	0.32
KLX04	489.49	489.50	Quartz monzodiorite	0.21
KLX04	489.50	489.53	Quartz monzodiorite	0.09
KLX04	489.53	489.58	Quartz monzodiorite	0.19
KLX04	489.60	489.61	Quartz monzodiorite	0.21
KLX04	489.61	489.62	Quartz monzodiorite	0.16
KLX04	489.62	489.65	Quartz monzodiorite	0.15
KLX04	489.65	489.70	Quartz monzodiorite	0.05
KLX04	489.73	489.74	Quartz monzodiorite	0.22
KLX04	489.74	489.75	Quartz monzodiorite	0.31
KLX04	489.75	489.78	Quartz monzodiorite	0.10
KLX04	489.78	489.83	Quartz monzodiorite	0.10
KLX04	499.70	499.73	Quartz monzodiorite	0.10
KLX04	519.84	519.87	Fine-grained granite	0.28
KLX04	539.68	539.71	Quartz monzodiorite	0.12

Borehole	Secup	Seclow	Rock_type	Porosity (%)
KLX04	559.69	559.72	Ävrö granite	0.33
KLX04	579.73	579.76	Ävrö granite	0.43
KLX04	600.37	600.40	Ävrö granite	0.27
KLX04	620.02	620.05	Ävrö granite	0.39
KLX04	640.02	640.05	Ävrö granite	0.29
KLX04	659.81	659.84	Ävrö granite	0.33
KLX04	680.77	680.80	Quartz monzodiorite	0.09
KLX04	700.20	700.23	Quartz monzodiorite	0.26
KLX04	718.21	718.24	Fine-grained granite	0.22
KLX04	718.24	718.27	Fine-grained granite	0.22
KLX04	718.27	718.30	Fine-grained granite	0.22
KLX04	719.37	719.40	Fine-grained granite	0.26
KLX04	740.40	740.43	Ävrö granite	0.25
KLX04	759.83	759.86	Ävrö granite	0.22
KLX04	780.73	780.76	Ävrö granite	0.20
KLX04	800.02	800.05	Ävrö granite	0.15
KLX04	820.90	820.93	Ävrö granite	0.23
KLX04	840.17	840.20	Ävrö granite	0.22
KLX04	860.28	860.31	Fine-grained diorite-gabbro	0.16
KLX04	880.25	880.28	Ävrö granite	1.45
KLX04	899.89	899.92	Ävrö granite	0.41
KLX04	920.40	920.43	Ävrö granite	0.80
KLX04	939.77	939.80	Ävrö granite	0.79
KLX04	978.72	978.75	Ävrö granite	0.33

Table A1-4. Porosity data from KLX06.

Borehole	Secup	Seclow	Rock_type	Porosity (%)
KLX06	402.41	402.44	Granite	4.19

Appendix 2

Formation factors and associated porosities

Laboratory and in situ formation factors (F_m), and porosities measured on samples used in laboratory formation factor measurements.

Table A2-1. Formation factor and porosity data from KLX02. Normal text refers to samples where the laboratory data originates from /Börjesson and Gustavsson 2005/ and italic text refers to samples where the laboratory measurements are from /Löfgren 2001/. Values for the formation factor given within parenthesis corresponds to preliminary values in through diffusion experiments where steady state not yet has been obtained.

Borehole length (m)	F_m lab (electrical resistivity)	F_m lab (through-diffusion)	F_m in situ (electrical resistivity)	Rock type	Porosity %
201.89	8.33E–05			Ävrö granite	0.30
216.70		5.2E–5		Ävrö granite	0.23
216.71		(2.3E–5)		Ävrö granite	0.13
216.74		(1.4E–5)		Ävrö granite	0.15
216.80		6.1E–5		Ävrö granite	0.21
216.81		(2.6E–5)		Ävrö granite	0.19
216.84		(1.5E–5)		Ävrö granite	0.16
216.91		7.5E–5		Ävrö granite	0.33
216.92		(3.5E–5)		Ävrö granite	0.21
216.95		(1.5E–5)		Ävrö granite	0.19
220.11	1.10E–04			Ävrö granite	0.36
235.02		3.1E–4		Ävrö granite	0.36
235.05		2.9E–4		Ävrö granite	0.39
235.08		3.2E–4		Ävrö granite	0.39
239.88	1.85E–04			Ävrö granite	0.28
258.96		(4.6E–5)		Ävrö granite	0.23
280.01	7.34E–05			Ävrö granite	0.19
299.79	1.01E–04			Ävrö granite	0.21
320.04	8.58E–05			Ävrö granite	0.13
339.95	1.52E–04			Ävrö granite	0.17
349.16	7.68E–05			Ävrö granite	0.29
349.21	1.58E–04			Ävrö granite	0.29
349.77	8.67E–05			Ävrö granite	
350.62	1.41E–04		6.89E–05	Ävrö granite	0.38
350.66	1.19E–04		6.95E–05	Ävrö granite	0.31
351.03	2.06E–04		6.83E–05	Ävrö granite	
351.35	1.13E–04			Ävrö granite	0.27
351.4	1.90E–04		8.11E–05	Ävrö granite	0.32
352.53	1.07E–04		6.58E–05	Ävrö granite	0.27
352.57	1.08E–04		5.77E–05	Ävrö granite	0.27
353.03	1.11E–04		5.13E–05	Ävrö granite	
353.56	1.24E–04			Ävrö granite	0.28

Borehole length (m)	F_m lab (electrical resistivity)	F_m lab (through-diffusion)	F_m in situ (electrical resistivity)	Rock type	Porosity %
353.57	1.30E–04		5.51E–05	Ävrö granite	0.26
354.03	1.99E–04		4.72E–05	Ävrö granite	
354.8	1.07E–04		4.37E–05	Ävrö granite	0.21
354.82	7.90E–05			Ävrö granite	0.19
354.84	6.62E–05			Ävrö granite	0.20
354.86	7.62E–05			Ävrö granite	0.20
354.88	8.70E–05			Ävrö granite	0.21
354.89	7.51E–05		3.35E–05	Ävrö granite	0.19
354.92	3.83E–05			Ävrö granite	0.18
354.93	2.87E–05			Ävrö granite	0.15
354.95	2.50E–05			Ävrö granite	0.14
354.97	2.09E–05			Ävrö granite	0.16
354.99	3.19E–05			Ävrö granite	0.15
355.01	2.72E–05		3.15E–05	Ävrö granite	0.16
355.03	2.98E–05			Ävrö granite	0.16
355.05	3.23E–05			Ävrö granite	0.14
355.07	2.55E–05			Ävrö granite	0.15
355.08	2.64E–05			Ävrö granite	0.14
355.1	3.17E–05			Ävrö granite	0.17
355.12	2.27E–05			Ävrö granite	0.16
355.14	3.00E–05			Ävrö granite	0.14
355.16	2.93E–05			Ävrö granite	0.14
355.18	2.80E–05			Ävrö granite	0.15
358	1.17E–04		4.65E–05	Fine-grained diorite-gabbro	0.25
359.05	1.99E–04		6.51E–05	Ävrö granite	0.33
360.46	2.58E–04		9.46E–05	Ävrö granite	0.25
362	1.54E–04		1.04E–04	Ävrö granite	0.32
362.06	1.86E–04		1.08E–04	Ävrö granite	0.35
363.22	1.34E–04			Ävrö granite	0.26
363.29	1.34E–04		9.61E–05	Ävrö granite	0.27
364.3	3.00E–04			Ävrö granite	1.05
365.79	1.67E–04			Ävrö granite	0.3
365.85	1.11E–04		9.65E–05	Ävrö granite	0.29
367.12	2.62E–04		9.66E–05	Ävrö granite	0.32
369.08	1.94E–04			Ävrö granite	0.34
369.09	3.52E–04		9.90E–05	Ävrö granite	0.3
371.66	2.95E–04		1.13E–04	Ävrö granite	0.43
372.77	2.12E–04		9.79E–05	Ävrö granite	0.3
372.84	3.23E–04			Ävrö granite	0.34
373.93	3.03E–04		9.93E–05	Ävrö granite	0.32
373.94	2.70E–04			Ävrö granite	0.32
375.05	3.31E–04		7.83E–05	Ävrö granite	0.31
375.07	3.75E–04		7.47E–05	Ävrö granite	0.3
376.06	3.49E–04			Ävrö granite	0.32
376.11	3.83E–04		1.10E–04	Ävrö granite	0.33
378.13	2.87E–04			Ävrö granite	0.37

Borehole length (m)	F_m lab (electrical resistivity)	F_m lab (through-diffusion)	F_m in situ (electrical resistivity)	Rock type	Porosity %
378.17	2.81E–04			Ävrö granite	0.35
381.64	1.42E–04			Ävrö granite	0.3
381.71	1.37E–04		7.87E–05	Ävrö granite	0.31
383.29	1.13E–04			Ävrö granite	
383.9	1.12E–04		5.12E–05	Ävrö granite	0.28
383.94	9.85E–05			Ävrö granite	0.25
384.41	2.31E–05			Ävrö granite	0.13
384.44	1.52E–05			Ävrö granite	0.08
386.07	7.76E–05			Fine-grained diorite-gabbro	0.38
386.11	6.70E–05			Fine-grained diorite-gabbro	0.22
387.78		(9.4E–5)		Fine-grained diorite-gabbro	0.36
388.75	2.48E–05			Fine-grained diorite-gabbro	0.16
390.37	1.38E–04		4.79E–05	Ävrö granite	0.29
390.43	6.21E–05			Ävrö granite	0.3
392.4	1.18E–04		5.24E–05	Ävrö granite	0.31
392.46	8.96E–05		4.73E–05	Ävrö granite	0.32
395.51	1.19E–04		5.45E–05	Ävrö granite	0.34
395.59	1.34E–04		5.73E–05	Ävrö granite	0.33
398.33	1.66E–04			Ävrö granite	0.3
398.38	1.48E–04			Ävrö granite	0.3
420.02	9.90E–05			Ävrö granite	0.25
440.21		(7.5E–6)		Ävrö granite	0.15
459.69	7.76E–05			Ävrö granite	0.38
480.02	1.15E–04			Ävrö granite	0.40
499.95	8.03E–05			Ävrö granite	0.25
519.63	1.26E–04			Ävrö granite	0.21
540.03	9.65E–05			Ävrö granite	0.29
560.72	2.15E–04			Ävrö granite	0.43
579.77	8.65E–05			Ävrö granite	0.30
600.19		(5.6E–5)		Ävrö granite	0.27
620.77	2.93E–04			Ävrö granite	0.34
639.93	6.03E–04			Ävrö granite	0.42
680.83	9.44E–05			Ävrö granite	0.27
682.34		(5.6E–6)		Fine-grained dioritoid	0.06
682.37		(5.6E–6)		Fine-grained dioritoid	0.06
682.40		(5.6E–6)		Fine-grained dioritoid	0.12
700.15		(7.0E–6)		Fine-grained dioritoid	1.49
722.4	1.28E–04			Fine-grained dioritoid	
725.07	6.27E–04			Fine-grained dioritoid	
728.28	1.91E–04			Fine-grained dioritoid	
731.03	1.48E–04		2.58E–05	Ävrö granite	
732.43	1.39E–04			Ävrö granite	
732.47	9.02E–05			Ävrö granite	0.48
738.67	1.57E–04			Ävrö granite	
739.92	3.96E–04		1.01E–05	Ävrö granite	
743.23	8.68E–05		3.23E–05	Ävrö granite	

Borehole length (m)	F_m lab (electrical resistivity)	F_m lab (through-diffusion)	F_m in situ (electrical resistivity)	Rock type	Porosity %
750.16	3.18E–05			Ävrö granite	
752.97	1.62E–04		3.27E–05	Ävrö granite	0.36
755.84	1.26E–05			Ävrö granite	
757.4	8.73E–05		2.63E–05	Fine-grained dioritoid	
760.11	1.46E–04			Ävrö granite	
760.86	1.19E–04			Ävrö granite	
770.96	2.43E–04		1.57E–05	Ävrö granite	
775.44	1.13E–04		2.21E–05	Fine-grained diorite-gabbro	
776.58	1.93E–04		2.32E–05	Ävrö granite	
776.62	7.48E–05			Ävrö granite	0.30
787.23	2.80E–04			Fine-grained diorite-gabbro	
791.59	1.24E–04			Ävrö granite	
796.11	1.58E–04			Ävrö granite	
796.14	9.79E–05			Ävrö granite	0.46
839.39	2.55E–05			Fine-grained diorite-gabbro	0.15
859.70	1.57E–04			Ävrö granite	0.42
898.04	1.10E–06			Fine-grained dioritoid	0.04
921.15	9.20E–06			Fine-grained dioritoid	0.07
938.42	2.03E–04			Ävrö granite	0.39
959.56	1.36E–04			Ävrö granite	0.32
979.92	2.92E–04			Ävrö granite	0.41
998.20	3.95E–05			Ävrö granite	0.25

Table A2-2. Formation factor and porosity data from KLX02A. Normal text refers to samples where the laboratory data originates from /Börjesson and Gustavsson 2005/ and italic text refers to samples where the laboratory measurements are from /Löfgren 2001/. Values for the formation factor given within parenthesis correspond to preliminary values in through diffusion experiments where steady state not yet has been obtained.

Borehole length (m)	F_m lab (electrical resistivity)	F_m lab (through-diffusion)	F_m in situ (electrical resistivity)	Rock type	Porosity %
110.4	7.62E–05			Ävrö granite	0.24
130.55	2.23E–04			Ävrö granite	0.46
149.56	7.91E–05			Ävrö granite	0.27
169.66	7.50E–05			Granite	0.38
190.62	8.04E–05			Ävrö granite	0.39
209.72	5.42E–05			Ävrö granite	0.36
236.78	4.28E–04			Ävrö granite	0.99
256.72	9.01E–05			Ävrö granite	0.43
277.66		(1.1E–5)		Fine-grained Dioritoid	0.39
297.06	1.80E–04			Ävrö granite	0.89
317.19	2.46E–04			Ävrö granite	0.36
337.55	9.35E–05			Ävrö granite	0.22

Borehole length (m)	F_m lab (electrical resistivity)	F_m lab (through-diffusion)	F_m in situ (electrical resistivity)	Rock type	Porosity %
357.06	3.99E–05			Ävrö granite	0.36
380.78	1.95E–04			Ävrö granite	0.63
400.72	2.70E–05			Quartz monzodiorite	0.19
419.95	3.06E–04			Granite	0.84
460.09	1.37E–05			Quartz monzodiorite	0.12
479.82	7.67E–05			Quartz monzodiorite	0.21
489.50		(5.2E–5)	2.02E–5	Quartz monzodiorite	0.09
489.53		(6.6E–5)	2.14E–5	Quartz monzodiorite	0.19
489.62		(3.1E–5)		Quartz monzodiorite	0.15
489.65		(8.0E–6)	2.23E–5	Quartz monzodiorite	0.05
489.75		(5.6E–6)	2.19E–5	Quartz monzodiorite	0.10
519.84	3.63E–05		2.55E–05	Fine-grained granite	0.28
539.68	2.04E–05			Quartz monzodiorite	0.12
559.69	6.75E–05			Ävrö granite	0.33
579.73	2.38E–04			Ävrö granite	0.43
600.37	5.36E–05			Ävrö granite	0.27
620.02	5.09E–05			Ävrö granite	0.39
640.02	5.76E–05			Ävrö granite	0.29
659.81	4.17E–05			Ävrö granite	0.33
680.77	1.35E–05			Quartz monzodiorite	0.09
700.2	9.71E–06			Quartz monzodiorite	0.26
719.38		(1.3E–5)		Fine-grained granite	0.26
740.4	1.04E–04			Ävrö granite	0.25
759.83	6.72E–05		7.12E–05	Ävrö granite	0.22
780.73	2.92E–05			Ävrö granite	0.20
800.02	7.88E–05		9.37E–06	Ävrö granite	0.15
820.9	1.89E–04			Ävrö granite	0.23
840.17	9.58E–05		1.86E–05	Ävrö granite	0.22
860.28	1.94E–05			Fine-grained diorite-gabbro	0.16
880.25	2.74E–04			Ävrö granite	1.45
899.89	2.91E–04			Ävrö granite	0.41
920.40		(1.9E–4)		Quartz monzodiorite	0.80
939.77	2.53E–04			Ävrö granite	0.79
978.72	1.76E–04		4.50E–05	Ävrö granite	0.33